Catalytic Combustion and NO Formation of Natural Gas

by

Huixiu Qi

A thesis
presented to the University of Waterloo
in fulfillment of the
thesis requirement for the degree of
Master of Applied Science
in
Mechanical Engineering

Waterloo, Ontario, Canada, 2014

AUTHOR'S DECLARATION

I hereby declare that I am the sole author of this thesis. This is a true copy of the thesis, including any required final revisions, as accepted by my examiners.

I understand that my thesis may be made electronically available to the public.

Abstract

As the world energy demand increases and the utilization of non-traditional fossil fuels becomes more attractive, natural gas, from shale gas and in gaseous and liquefied forms, becomes one of the most promising alternative fuels nowadays. The natural gas offers lower fuel production and transportation costs, a lower carbon content, a higher combustion efficiency and a greater applicability to most of existing power plants and combustion engines. Challenges exist, especially in improving its ignition characteristics and to further reduce its greenhouse gas and particulate matter emissions.

To overcome these restraints, hydrogen addition, catalyst modification and fuel lean combustion have been investigated recently. In this thesis, the ignition and emission properties of methane and its mixtures with hydrogen additive are first studied in the mini-channel reactor. Numerical investigations have been performed using the CHEMKIN PRO software for pure methane and the mixtures of methane and hydrogen in non-catalytic and catalytic combustion. These effects of the hydrogen fractions, Pt-catalyst, wall temperature and inlet conditions on the ignition delay and NO formation are investigated. Available gas phase kinetics and heterogeneous surface reaction mechanisms in the literature are implemented and analyzed.

As the second part of this thesis, natural gas combustion on a counter-flow burner is investigated experimentally and numerically, with a focus on NO formation. The NO profiles, measured by the FT-IR spectroscopy, are compared with model results from CHEMIKIN and with the GRI-Mech 3.0 mechanism. The formation mechanism of NO and effects of the different fuel/oxidizer ratios on the NO formation are investigated.

Acknowledgements

I am very thankful to my supervisor Prof. John Z. Wen for his continuoussupport and guidance during my master study. I feel thankful to him for his patience, insightful advice and suggestions. It is a great pleasure to work with Prof.Wen.

The financial support has been provided by Natural Sciences and Engineering Research Council of Canada (NSERC),Networks of Centres of Excellence: BioFuelNET and Cestoli Chemical Inc. I would specially thank Dr. Henry Zhu and Mr. Samuel Xiong for their support and regular meetings and discussions.

I would specially thank Prof. Zhongchao Tan and Prof. Robert Varin forbeing on my thesis committee.

Thanks to my colleague Kang Pan for designing the burner and providing help on the experiments.

Thanks to my colleague Abhishek Raj for his suggestions and help on the experimental instruments.

Thanks to my colleague Ahmad El Sayed for his suggestions on my CHEMKIN modeling work.

I would also like to thank Tao Xu, Tracey Zhou, Saleh Lavaee, JohnRawlins, Jinhee Kang and SanamAtashinfor their help.

Thanks to Jason Benninger and Engineering Machining shop for technical support.Finally, I would like to thank my parents and sister for their love, support and encouragement.

Dedication

This thesis is dedicated to my parents, who support me each of the step.

Table of Contents

List of Figures

List of Tables

Chapter 1
Introduction

1.1 Motivation

Coal and petroleum fuel have been used widely as an un-replaceable energy resource in human being's history. A number of issues associated with their uses are well known including the energy security and environmental impacts, such as producing carbon monoxide (CO), carbon dioxide ($CO_{2)}$, nitrogen oxides (NO_x), sulfur oxide (SO_x) and particulate matters. Thus, cleaner energy resources have been sought, with options of developing environmental-friendly system and using cleaner fuel sources. There are several fuels viewed as alternative energy sources for this purpose, such as methane, hydrogen and biofuels[1].

Natural gas mainly consists of methane (above 96%), which is one of the most promising alternative fuels. It offers lower fuel cost, lower carbon content, higher efficiency and higher applicability to most of existing power plants and combustion engines. However, its ignition temperature is relatively high and the flame propagation rate is considerably slow[2-4].In addition, the emissions from natural gas from industrial systems are still fairly high.

To improve the natural gas combustion efficiency and reduce emissions, numerous of techniques have been developed. Among them, fuel lean operation, hydrogen addition and catalysts addition have shown a good performance to overcome these limitations.

Fuel lean operation is widely used for industrial combustion processes. It can significantly reduce the pollutant emissions, especially NO_x. However, NO_x formation is still dependent on the fuel/oxidizer ratio under fuel lean operations. To investigate the effect of fuel/oxidizer ratio, the study of natural gas combustion with different fuel/air ratios is necessary.

Compared with methane, hydrogen, on the other hand, is viewed as an important alternative fuel for the future as its combustion products are nearly environmentally friendly[5]. Hydrogen combustion exhibits a low ignition temperature and a high flame

propagation rate. However, most hydrogen is still obtained from fossil fuels and the use of hydrogen indirectly links to using fossil fuels. Another issue for using hydrogen is how to deliver and store hydrogen. Because hydrogen has a fast diffusion rate and a great flammability, which makes it easy to explode[6]. A combination of methane and hydrogen has a possibility to overcome some limitations of the individual gases. The recently proposed power-to-fuel energy management scheme utilizes electricity to produce hydrogen which is then injected into the natural gas pipeline[7]. It is therefore interesting to investigate an alternative way to use these two fuels together by adding a certain amount of hydrogen into natural gas.

Considering to more effectively reduce the NO_x emission and improve methane combustion performance, introducing catalysts into combustion system can be an solution. The most commonly used catalysts include the Platinum (Pt) catalyst for combustion reactors. This technology can reduce emissions and improve the combustion process by providing a low activation energy and a low reaction temperature[8-11]. It has become interesting to investigate the effects of catalysts on combustion of methane and hydrogen mixtures the formation levels of NO_x from these mixtures. Moreover, analysis of the catalytic mechanism is important to provide guidance for the future technology development.

1.2 Objectives

The overall objective in this work is to study the effects of hydrogen and catalyst on combustion characteristics and emissions of natural gas (methane). For this purpose, the experimental and numerical studies on natural gas combustion are conducted.

1. To study the effects of hydrogen and Pt-catalyst on the ignition delay, intermediate species concentration, and NO_x emission through simulating the methane combustion process in a flow reactor with the CHEMKIN software.
2. To develop experimental procedures for characterizing methane combustion on a counter-flow burner and to develop a nitric oxide (NO) emission measurement technique using FTIR.

3. To quantify the fuel/oxidizer ratio effects on the NO production from methane combustion on the counter-flow burner and to investigate the NO formation pathway by modeling the same flame. These steps are necessary for the next-step study about the effects of hydrogen and catalysts addition on combustion properties and NOx formation from the counter-flow burner.

Chapter 2
Literature Review

Natural gas, which mainly consists of methane, is an abundant petroleum product. It is considered to be cleaner than other fossil fuels due to its low nitrogen and sulfur containing. The gas emissions of different fuels are shown in Figure 2-1[12][13].

Natural gas is a gas mixture consisting mainly of methane (CH_4), some higher alkanes and less percentage of carbon dioxide and nitrogen. The typical components of natural gas can be shown as Table 2-1[14, 15].

Table 2-1 General components of natural gas

Component	Range (mol %)
Methane (CH_4)	83.0-97.0
Ethane (C_2H_6)	1.5-7.0
Propane (C_3H_8)	0.1-1.5
Butane (C_4H_{10})	0.02-0.6
Pentane (C_5H_{12})	≤0.08
Hexanes plus (C_6+)	≤0.06
Nitrogen (N_2)	0.2-5.5
Carbon dioxide (CO_2)	0.1-1.0
Oxygen (O_2)	0.01-0.1
Hydrogen (H_2)	≤0.02

2.1 Gas emissions of natural gas combustion

Methane is the main component of natural gas,mainly used in energy generation by burning as a fuel. It is the simplest alkane. It is colorless, odorless and flammable. Methane molecule has four C-H bonds and only one carbon atom. Thus, the production of CO_2, which is viewed to be one of greenhouse gas, per unit of produced energy is the lowest by natural gascombustion[9]. In the complete combustion of methane, the products should be ideally only carbon dioxide and water. The complete methane combustion can be showed as the overall reaction by the equation[16]:

$$\boldsymbol{CH_4 + 2O_2 \rightarrow CO_2 + 2H_2O,\ \Delta H_{298K} = -802.7 KJ/mol} \qquad \textbf{(2-1)}$$

But in most cases, pollutant components are produced during incomplete combustion process or high temperature operations. The main pollutant products of methane combustion are carbon monoxide, nitrogen oxides and soot.

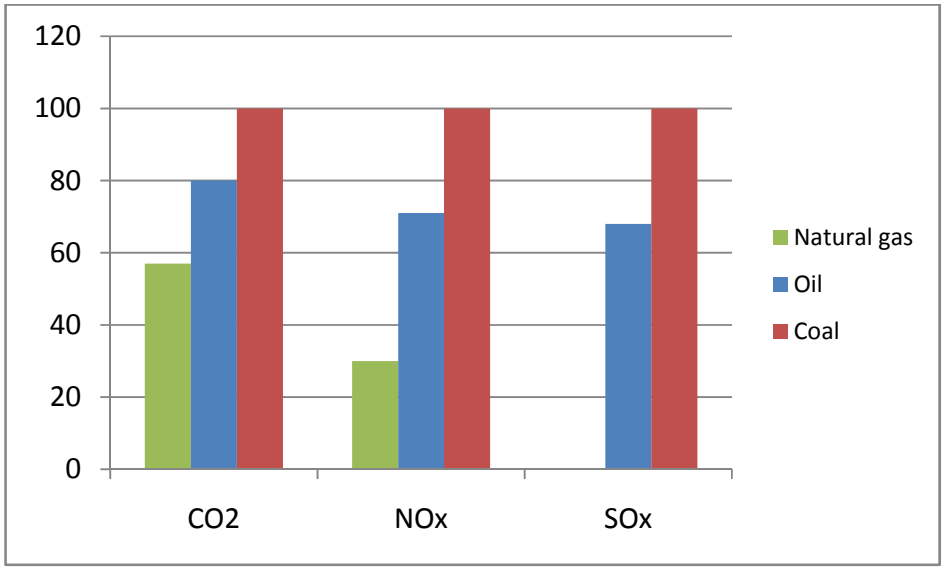

Figure 2-1Gas emission comparisons of coal, oil and natural gas combustion (coal emission is viewed as 100%)based on data from [12][13]

2.1.1 CO emission

Carbon monoxideis produced by incomplete combustion. It is one of the most harmful air pollutants. It is very toxic and harmful to people's health. When people inhaled carbon monoxide, it can react with the blood's hemoglobin to produce carboxyhemoglobin (COHb) which is very stable. The COHb is produced in red blood cells and hinders delivery of oxygen to the body[17].

During hydrocarbon combustion process, CO is the major intermediate before CO_2 formation. In general, the hydrocarbons would be oxidized to CO first, and then CO_2 is formed through further oxidation.

$$\mathbf{C_xH_y + O_2 = xCO + \frac{n}{2}H_2O} \qquad \textbf{(2-2)}$$

$$\boldsymbol{2CO + O_2 = CO_2} \qquad \textbf{(2-3)}$$

The CO emission from natural gas combustion in diesel engine was studied by Abdelaal and Hegab[18]. The CO levels were obtained for different operating modes. CO emissions of conventional diesel mode are lower than those from dual-fuel mode; in addition, the CO emissions can be reduced slightly with the application of exhaust gas recirculation (EGR). Wang et al.[19] studied the homogeneous combustion of fuel ultra-lean methane/air mixtures. The CO and CO_2 formation pathway was carefully studied. The results indicated that most of methane is oxidized to CO first and CO is further oxidized to CO_2. However, they also found a little methane was directly oxidized to CO_2 at low temperatures.

2.1.2 Particulate matter emission

Particulate Matter (PM) is one of the most important pollutants produced during combustion process. They are typically solid particles or liquid droplets with small diameters[20].Particles generated from combustion process have gained lots of interest due to their direct negative effects on human's health and environments. PM includes smoke, ash, dust and soot, in general. In recent years, soot formation has attracted more attentions by researchers as it is one of the major PM sources.

Soot is small carbon particles produced in the process of incomplete combustion of hydrocarbons. There are several mechanisms of soot formation, including polyacetylenes, ionic species and polycyclic aromatic hydrocarbons (PAH) as the key precursors of soot formation. Among them, PAH as precursor is most acceptable mechanism until now. There are several steps in this mechanism[20, 21]:

a) The fuel molecules are broken down to smaller hydrocarbon molecules and free radicals (such as CH, C_2H_2 and C_2H_3, etc) via pyrolysis or oxidation reactions.

b) The aromatic rings are formed by the generated small hydrocarbon molecules and free radicals. The typical formed ring molecules are 6-membered aromatic ring (benzene and phenyl) or 5-membered aromatic ring (cyclopentadienyl or cyclopentatriene). This step is usually viewed as rate determining step.

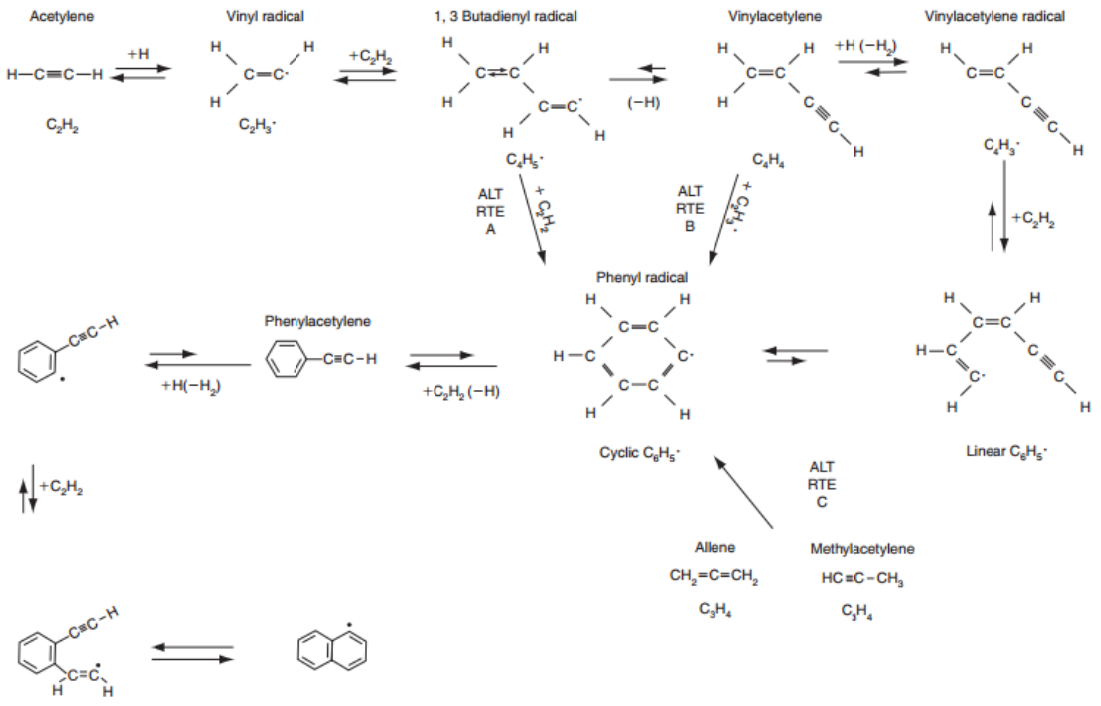

Figure 2-2 General mechanism for soot formation[22]

c) After small aromatic rings are formed, they will grow into larger aromatic rings which are PAH by C_2H_2 addition and H_2 abstraction.

d) The soot particles (diameter<1nm) are formed by coagulate the PAHs. Then, larger particles are generated by continuous coagulation and growth reaction on the surface.

e) The soot particles are further oxidized by O_2 or other oxidizers to form the final sort emissions from the combustion process.

Marinov et al. [23]studied the chemical kinetic paths for soot formation of the methane opposed flow diffusion flame. In their study, the numerical model was compared with experimental measurements and showed reasonable agreement for the large hydrocarbon aliphatic compounds, aromatics, two-ring PAHs, and three-ring PAHs. However, the numerical prediction of the four-ring PAHs doesn't consistent with experimental measurement. Their work also indicated that there are multipathways leading to aromatic and PAH formation according to the flame (premixed or diffusion) and hydrocarbon type. The soot formation from methane/air diffusion flame was investigated by Sivathanu and Gore[24]. Their model showed that the oxidation of soot by OH radicals dominates the soot emission from the flame; the local radiative heat gain or loss influences the rates of soot nucleation, formation and oxidation significantly.

2.1.3 NO emission

Nitrogen oxides, described by NO_x, are considered to be very important air pollutants. NO_x include nitric oxide (NO) and nitrogen dioxide ($NO_{2)}$. They can lead to acid rain, fog mist as well as damage ozone layer and harm the breathing system of human and animals. Combustion with the presence of oxygen and nitrogen at high temperature can lead to NO_x production. Nitric oxide NO is formed initially in homogeneous combustion. Then, NO can continually react with oxygen to form nitrogen dioxide NO_2.In combustion process, nitrous oxide (N_2O) can be produced and it is another source of NO formation and considered as an important greenhouse gas because of its stability.

There are mainly three pathways for NO_x formation [9, 25]: thermal NO_x, prompt NO_x and fuel NO_x.

a) Thermal NO_x is produced by the reaction of nitrogen and oxygen in the air under high temperatures. The principle reactions producing thermal NO_x are shown as Equation 2-1 to 2-3. The reactions are reversible and the mechanism is from Zeldovich[26]. Thermal NO_x is usually formed at the temperature higher than 1600°C. The production increases significantly with increasing residence time and it is strongly affected by flame temperature. Higher flame temperature leads to more thermal NO_x production.

$$\boldsymbol{N_2 + O = NO + N} \quad \textbf{(2-4)}$$

$$\boldsymbol{N + O_2 = NO + O} \quad \textbf{(2-5)}$$

$$\boldsymbol{N + OH = NO + H} \quad \textbf{(2-6)}$$

b) Prompt NO_x is formed by fast coupling of nitrogen in the air with radicals (C, CH and CH_2 et al.) formed at the flame front. The produced nitrogen species, such as NH, HCN, H_2CN and CN, can be oxidized to NO. Prompt NO_x is mainly produced at fuel rich conditions and at moderate temperatures. In general, the prompt NO_x production in fuel lean combustion is very little.

c) Fuel NO_x is formed by the oxidation of nitrogen compounds present in the fuel. The nitrogen compounds in the fuel release free radicals and ultimately form N_2 or NOduring combustion process. Fuel NO_x production requires nitrogen-bearing fuels, such as coal and oil. There are almost no nitrogen compounds in natural gas, so fuel NO_x is rarely generated in natural gas combustion process.

There is little fuel NO and prompt NO produced during natural gas combustion under fuel lean conditions. Because natural gas mainly consists of methane and there is little nitrogen containing in the natural gas. Thus, thermal NO is the dominant path of NO_x production in most natural gas combustion devices.

The NO_x formation was numerically studied by Loffler et al[27]. In this study, a simplified model for thermal NO formation was developed by CFD calculations. The NO model, including thermal NO route, N_2O/NO and NNH route, was evaluated under a wide range of conditions. The variation of temperature showed that NO formation is primary from thermal mechanism with high temperature (>1600°C). Barlow et al. investigated the NO formation in laminar opposed flow partially premixed methane/air flames [28]. The major species, including N_2, O_2, CH_4, CO_2, CO, H_2O, OH and NO were measured by using non-intrusive techniques of Raman scattering and laser-induced fluorescence and compared with numerical modeling of reduced GRI-Mech 2.11[29] and 3.0[30] and detailed Miller mechanisms[31]. Three different fuel side equivalence ratios ϕ(1.8, 2.17 and 3.17) were employed. GRI-Mech 2.11 predicted reasonable results with measured NO from lean and near stoichiometric conditions, but it under-predicted the NO levels from fuel rich conditions. GRI-Mech 3.0 gave reasonable prediction for ϕ=1.8 flames, but over-predicted ϕ=2.17 or 3.17 flames. While, Miller mechanism only gave consistent results with ϕ= 3.17 flames.

2.2 Emission reduction techniques

Due to the increasing demand of energy from combustion process, large amount of pollutants are produced. To control the emissions generated from combustion process, a lot of technologies have been developed and studied in recent years.

2.2.1 Fuel to oxidizer ratio

Fuel/oxidizer ratio is one of the key parameters in the combustion process. It can affect the combustion performance and all the generated emissions. Fuel-lean operation is used to control the emissions, especially NO_x formation. In general, under fuel-lean operation can reduce NO_x a lot, but sometimes it can increase CO emissions and make the combustion process unstable.

Kesgin[32] investigated the excess air ratio effects on the natural gas combustion emissions. In the study, the excess air ratio varied from 1.55 to 2. The CO and hydrocarbon emissions were reduced while the excess air ratio increasing. NO formation was reduced as a

result of lower flame temperature. In addition, the fuel economy was improved by lean operation.

Kapaku[33] studied the effects of fuel/air ratio on the emissions by employing CHEMKIN's partial stirred reactor model with GRI-Mech3.0 mechanism. His work indicated that the NO_x emissions are strongly affected by the fuel/air ratios. The maximum values of NO_x were gained near the stoichiometric conditions; the minimum values of NO_x were gained under fuel lean conditions. And under fuel lean conditions, the NO_x levels would be reduced as increasing excess air ratios.

2.2.2 Hydrogen addition to methane combustion

Hydrogen is highly flammable and easy to burn. However, it is hard to store and deliver. Therefore, it is not a good idea to burn pure hydrogen as a fuel, but it is a good additive to improve the combustion of hydrocarbons due to its low ignition energy, high reactivity, high diffusivity and high flame propagation rate[34-36]. The recently proposed power-to-fuel energy management scheme utilizes electricity to produce hydrogen which is then injected into the natural gas pipeline [7]. For the safety and economic reasons, the maximum molar fraction of hydrogen was suggested to be less than 15% in the mixture[37].

Adding hydrogen to natural gas combustion was confirmed to promote ignition process and propagation rate, which subsequently decrease the combustion period and reduce the HC, CO and CO_2 emissions, compared with pure natural gas combustion. The effects on the NO_x emission of adding hydrogen to natural gas combustion have been evaluated in different engines under various operation conditions. It is found that when producing the same engine output power the NOx level increased with hydrogen addition[4, 5, 34, 35]. While, others found that hydrogen addition can contribute to NO_x reduction at the same flame velocities[36]. In engine studies, the NO_x emission resulting from hydrogen addition can be reduced by controlling the exhaust gas recirculation[38, 39].

Ma et al. studied the combustion properties of hydrogen enriched naturals gas in engines[40]. They found that the lean limit of natural gas combustion in the engine was

extended by hydrogen addition. And the thermal efficiency of natural gas engine can be improved by adding hydrogen into combustion system. Combustion of hydrogen and natural gas blends in spark ignition engine was also studied[1, 4, 34]. Natural gas combustion was enhanced with hydrogen addition. By adding hydrogen into natural gas, the CO and HC emissions decreased a lot while NO_x emissions increased significantly. Researchers also conducted experiments on hydrogen and methane combustion in shock tube reactors[41]. Results showed that hydrogen addition has the effect on reducing ignition delay time.

Cimino et al. [42] analyzed the effects of H_2, CO and C_3H_8 on the methane catalytic combustion over $LaMnO_3$ monolith. All the three gases can promote methane ignition. H_2 and C_3H_8 enhanced CH_4 gas phase oxidation and CO can promote CH_4 heterogeneous reactions at low temperature thanks to its high reactivity. Zhao et al. [36] studied hydrogen enriched methane combustion in a quartz reactor. Their work showed that hydrogen can decrease ignition temperature and burn off temperature of methane and the ignition temperature can be decreased up to 180°C when H_2/CH_4 was 2.5. Deutschmann et al. [8] studied the catalytic combustion of hydrogen and methane mixtures on monolith platinum. Their experiments showed that the main effect of hydrogen is to provide heat to reach methane's ignition temperature. Their modeling work studied the kinetic effect of hydrogen addition by employing only surface mechanisms and indicated that hydrogen can consume the oxygen on the platinum surface which inhibits methane adsorption and oxidation.

2.2.3 Exhaust gas recirculation (EGR)

Exhaust gas recirculation (EGR) is a technique developed for engines aimed to reduce pollutant emissions from combustion process. During the process, a portion of the exhaust gas from the engine is re-circulated back to the engine cylinders. Now, this technique is used widely for most engines to meet emissions standards.

The study presented by Abdelaal and Hegab investigate the combustion performance and emissions conditions from natural gas combustion in the diesel engine with EGA[3]. A single cylinder direct injection diesel engine was modified to dual-fuel mode. Natural gas mixed

with small amount diesel fuel was filled into the engine with different portions of EGR (5%, 10% and 20%). The results showed that EGR delayed the combustion ignition and reduced the pressure rise rate. For emissions, EGR can reduce the NO_x emissions significantly but reduce the HC and CO emissions only slightly.

The natural gas combustion performance and emissions from spark-ignition and compression-ignition engine was investigated[43]. It implied that high levels of NO_x emissions can be reduced with EGR operation, especially at high loads conditions for spark-ignition engines. For compression-ignition engines, uncooled EGR can speed up the combustion and improve combustion efficiency; it can also reduce HC, CO and NO_x at low to medium loads.

2.2.4 Catalytic combustion

Combustion process with catalysts addition is usually called catalytic combustion. In general, catalyst is used in small amounts relative to reactants and can modify or increase the rate of a reaction without being consumed in the process. It works to lower the reaction activation energy by providing an alternative pathway. Combustion is the process of burning, accompanied by the production of heat and light. Catalytic combustion normally refers a process which uses catalysts to improve desired oxidation reactions of fuel combustion to improve combustion efficiency and/or reduce the formation of undesired products[44, 45].

There are two main important advantages of catalytic combustion over homogeneous combustion of natural gas. Catalytic combustion of natural gas can occur at lower temperatures compared to homogeneous combustion of natural gas. The lower combustion temperature can lead to lower heat loss, less NO_x emissions; it is easier to control combustion systems with lower combustion temperature. Because of the obvious advantages, the interest of catalytic combustion technology has been increased significantly in recent years[10, 46-48]. Researchers are trying to use catalysts to improve methane combustion in power generation systems, reducing gas emissions and producing other products [9, 49, 50].

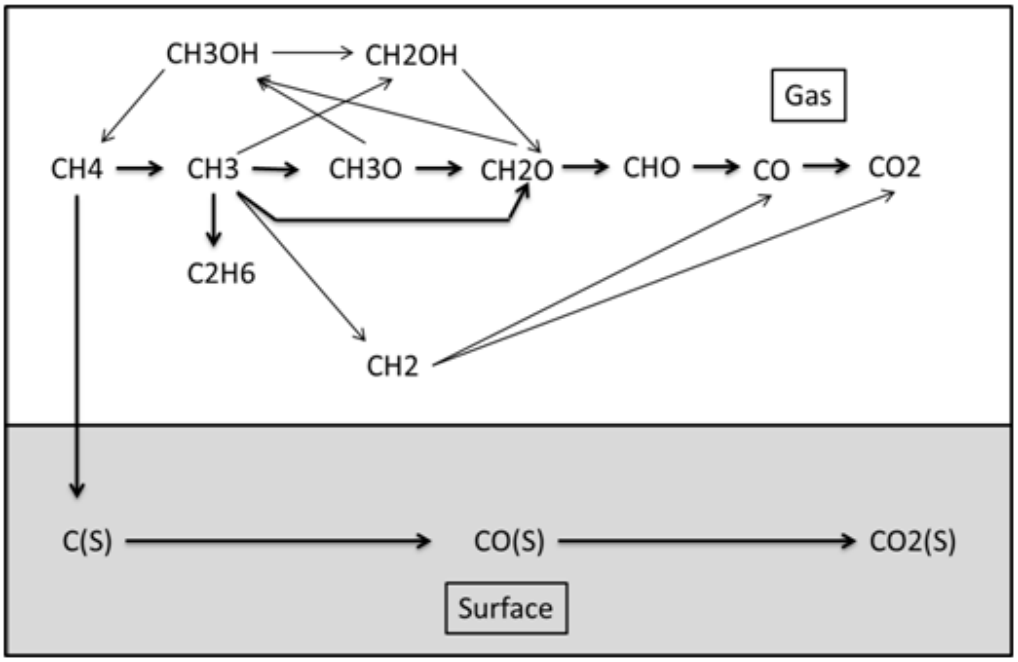

Figure 2-3 Scheme of simplified methane catalytic combustion process[45]

The effects of Pt and Pd based catalysts on hydrogen and methane combustion have been studied recently[8, 51]. During the studies, the fuel conversion, CO, CO_2 and NO_x emissions were analyzed. It was found the fuel conversions were improved and gas emissions were reduced by using the catalyst. Appel et al. [52] presented experimental and numerical study on the platinum catalyzed combustion in micro-channels of hydrogen and methane. They analyzed the coupling between homogeneous and catalytic mechanisms at various pressures and found the heterogeneous mechanisms have limited effects on homogeneous ignition. Schwiedernoch et al. [53] studied ignition process of methane catalytic combustion in catalytic monolith coated with Pt. It indicated that the ignition will occur at the outer channels and the heat generated will heat up the whole catalyst monolith. Then, ignition happened in the inner channels.

2.2.4.1 Catalytic combustion process

A simplified catalytic combustion process of methane is shown in Figure 2-3[54]. In the catalytic combustion process, there are several steps[45] in general:

a) Adsorption process. During this step, the reactants conduct mass transfer process from the homogeneous phase to the surface of catalyst and then diffuse into the catalyst pores.

b) Surface reactions. The reactant species have a series of chemical reactions with catalysts and each other on the surface of catalysts

c) Desorption process. The generated products desorb from the catalyst surface. The desorbed species will go into the homogeneous phase and continue reactions.

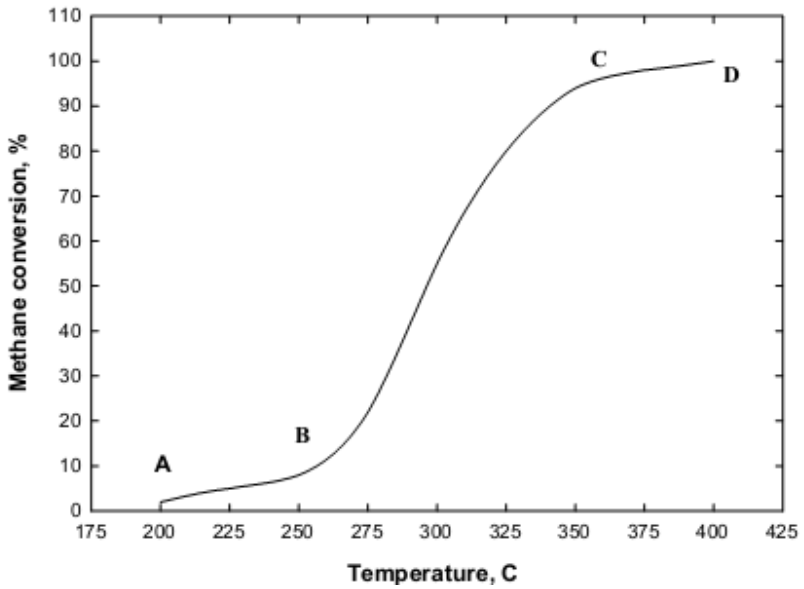

Figure 2-4 Conversion of methane in catalytic combustion vs. temperature[55]

Catalytic combustion produces a considerable amount of thermal energy with reactions going on and the temperature of reactants mixture would increase fast due to the large amount of released heat at the beginning of combustion. The rate of surface reaction respect to temperature is shown in Figure 2-4[55]. During A-B section, it is low temperature period

which lead to kinetics controlled reactions. With temperature increasing in B and C period, mass transfer is the dominant controlling factor for the reaction system due to the fast increasing reaction rate. Moving to C and D section, the homogeneous gas phase reaction becomes significant as well as the effects of mass and heat transfer.

2.2.4.2 Catalysts for methane combustion system

Various types of catalysts are designed for combustion systems. There are several main categories of catalysts in methane combustion process: noble metals, transition metal oxides and organic metal compounds.

In general, there are several necessary characteristics for a catalyst to be suitable for commercial applications[56]:

a) High selectivity for the desired products in order to reduce the cost for products separation.

b) High activity, which required low catalyst amount per unit of products to minimize the cost of catalysts.

c) Low price.

d) High mechanical strength, excellent heat transfer properties, thermal stability, and high attrition resistant.

Noble metals

Noble metals are used to improve methane catalytic combustion process. It is generally viewed that the activity of noble metals is higher than other catalysts[57]. Pt and Pd are the most commonly studied and used catalysts in combustion applications. The main advantage is that noble metals have higher catalytic site activity and better resistance of sulfur poisoning [58].However, noble metals are much more expensive than other oxides; the higher price is the most significant limitation of noble metal catalysts.

Pd-based catalyst is one of the most common used catalysts for methane combustion [9, 58, 59]. Compared to PtO_2, PdO can be easily transformed at a temperature lower than

1100K and remain stable. Thus, the activity of PdO is better than that of Pt, due to better stability of PdO. Using PdO can lead to higher conversions especially on the fuel lean conditions. In Salaun's study[60], in the case of the Pd catalyst for the reactant gas mixture of CH_4, CO, NO with trace of H_2 and CO_2, the reaction started at 250°C, ignition occurred at 325°C, and complete conversion of methane was reached at 400°C. These values for Pt catalyst were 450°C, 675°C and 900°C, respectively[60]. However, Pt catalysts show better ability of resistance to the poisons, such as water and sulfur, and they hardly sinter at low temperatures[61-63]. In a word, Pd catalysts are more active;while Pt catalysts are more stable and the pathway of Pt catalysts is much simpler than Pdcatalysts which undergo complex phase transformations due to temperature changes [64]. In addition, under some certain conditions Pt catalysts are proved to be more efficient. Kinetic studies showed that for deep oxidation of low alkanes (C1-C4) over Pd and Pt catalysts, Pt catalysts showed better performance[64]. It is also showed that Pt catalysts are more efficient that Pd for high conversions of methane combustion in the cases of stoichiometric or rich mixtures[65]. And it is thought that Pt catalysts are more important than Pd catalysts for the emissions control of natural fuels.

Metal oxides

Metal oxides are much cheaper compared to noble metals. Thus, applications of metal oxides are more desirable from the economic point[66-68]. However, their catalytic activity is lower. Perovskite metal oxides are the most commonly investigated and used among various types of metal oxides[69]. Perovskites are mixed metal oxides with face center cubic structure; they have many applications in the fields of transistors, fuel cells and superconductive materials. The general formula for these types of catalysts is ABO3. A is the rare earth element which is mostly responsible for the stability of structure and B is a transition metal which is mostly responsible for the catalytic activity. A has a dodecahedral coordination and B has a six-fold coordination. Among all the perovskites, LaMnO3 (B can also be Co, Fe and Ni) is considered to show good performance for methane combustion[70].

Organic metal compounds

The behavior of metals in flame system has been of interest for a long time. Recently, high temperature metal chemistry was used in the areas of nanoparticle synthesis, pollutant control, emission control and NO_x reduction techniques[71-76]. It is found that metal containing compounds can be used in flame inhibition and emissions control fields. Among all the metal compounds, iron pentacarbonyl($Fe(CO)_5$)showed great performance on controlling methane-air flames[69, 77, 78].

In most studies, $Fe(CO)_5$ is used as flame inhibitors in methane combustion system. The effect of $Fe(CO)_5$ on ignition was studied in flames of hydrocarbon mixtures[69]. It is found that $Fe(CO)_5$ had no obvious effect on ignition temperature. While, in shock-tube studies of methane combustion process, it is found that by adding $Fe(CO)_5$ (500, 1000, 2000 uL/L) the ignition time decreased compared to without the additive, which indicated that adding metal additive had a promotion effect on ignition delay[77]. The CO combustion system with $Fe(CO)_5$ tests showed that $Fe(CO)_5$ can significantly accelerate the CO consumption, which can promote CO emission reduction[75]. In addition, the effects of $Fe(CO)_5$ on burning velocity has been studied. It was showed that $Fe(CO)_5$ had a strong effect on reducing the burning velocity of hydrocarbon/air flames in nozzle burners, which can greatly affect the gas emissions. It was found the burning velocity reduced 25% by adding 100uL/L $Fe(CO)_5$ into methane-air flames at atmospheric pressure [69, 79].

Due to the effects on the flame velocities and emission control, $Fe(CO)_5$ has been of interest in recent combustion studies. But the mechanism and kinetics are still not clear.

2.2.4.3 Mechanism of methane catalytic combustion system

Reaction mechanisms can describe the complete combustion of different fuels at different conditions. There has been a lot of research on the gas-phase and surface-phase reaction mechanism and kinetics of methane combustion system[80-82].

Homogeneous mechanism

For the gas phase reaction mechanism, which is homogeneous pathway, the global reaction of fuel reacted with oxidizer can be expressed by Equation 1,

$$\boldsymbol{Fuel + Oxidizer = Products} \quad \textbf{(2-7)}$$

The global reaction can be broken down into the elementary reactions to understand the chemistry for the combustion process, as equations shown.

$$\boldsymbol{A + B \rightarrow C + D} \quad \textbf{(2-8)}$$

$$\boldsymbol{A \rightarrow B, A \rightarrow B + C} \quad \textbf{(2-9)}$$

$$\boldsymbol{A + B + M \rightarrow C + M} \quad \textbf{(2-10)}$$

In the equation, A and B are reactants; C and D are products; and M is an unreactive third-body in radical-radical reactions required to add or carry away the energy of the reaction. The elementary reaction rate can be expressed as Equation 5, 6 and 7.

$$\frac{\boldsymbol{d[A]}}{\boldsymbol{dt}} = -\boldsymbol{k_{bi}[A][B]} \quad \textbf{(2-11)}$$

$$\frac{\boldsymbol{d[A]}}{\boldsymbol{dt}} = -\boldsymbol{k_{uni}[A]} \quad \textbf{(2-12)}$$

$$\frac{\boldsymbol{d[A]}}{\boldsymbol{dt}} = -\boldsymbol{k_{ter}[A][B][M]} \quad \textbf{(2-13)}$$

In the equations, the reactants in brackets [] are the concentration and k is the rate coefficient.

From each elementary, the reaction mechanism can be expressed by Arrhenius equation:

$$\boldsymbol{k(T) = AT^{n} exp(-\frac{E_a}{RT})} \quad \textbf{(2-14)}$$

k(T): the rate coefficient;

A: pre-exponential factor (mol, cm^{-3},s);

T: temperature (C);

n: temperature coefficient;

E_a: activation energy (kcal/mol);

R: gas constant.

Reactions may proceed in both a forward and reverse direction. For this reason, the reaction should have a corresponding rate coefficient for the forward and reverse reaction, k_f and k_r. The equilibrium constant relates the forward and reverse rate coefficients and can be expressed as Equation 2-13.

$$\frac{A_f \exp\left(-\frac{E_f}{RT}\right)}{A_r \exp\left(-\frac{E_r}{RT}\right)} = \frac{k_f}{k_r} = K_c \qquad \textbf{(2-15)}$$

There are a lot of research on the homogeneous mechanism of methane combustion: GRI-Mech series mechanism (including GRI-Mech 1.2[83], GRI-Mech 2.11[29] and GRI-Mech3.0[30]); Miller-Bowman mechanism[31]; Lutz mechanism[84]; Smooke-Giovangigli mechanism[85]; UBC mechanism[86], etc. Among them, the GRI mechanisms are widely used. The most updated version is GRI-Mech 3.0 mechanism which includes 325 elementary chemical reactions and 53 species. It includes all important reactions for natural gas ignition, flame propagation and NO formation. The GRI-Mech 3.0mechanism has been validated for a wide range of combustion conditions [87-89].

Heterogeneous mechanism

The heterogeneous pathway has been mentioned in the former section, including adsorption, surface reaction and desorption processes. The general surface reactions can be expressed as the equations[25, 90]:

$$A_{ads} + B_{ads} \rightarrow product \qquad \textbf{(2-16)}$$

$$A_{ads} + B_{gas} \rightarrow product \qquad \textbf{(2-17)}$$

The reaction rates can also be calculated from Equation 2-12 and 2-13.

Based on the experimental and numerical study, various surface reaction mechanisms are developed on various catalysts. For methane combustion on platinum, an improved multi-step surface reaction mechanism is developed by Deutschmann[8].There are other mechanism schemes of methane combustion on Pt developed by other researchers, such as Chou et al.[91]. In both of their mechanism, it includes the adsorption of O_2 and CH_4 and intermediates including CO, H_2 and OH on the active sites, surface reaction and desorption of CO_2 and H_2O.

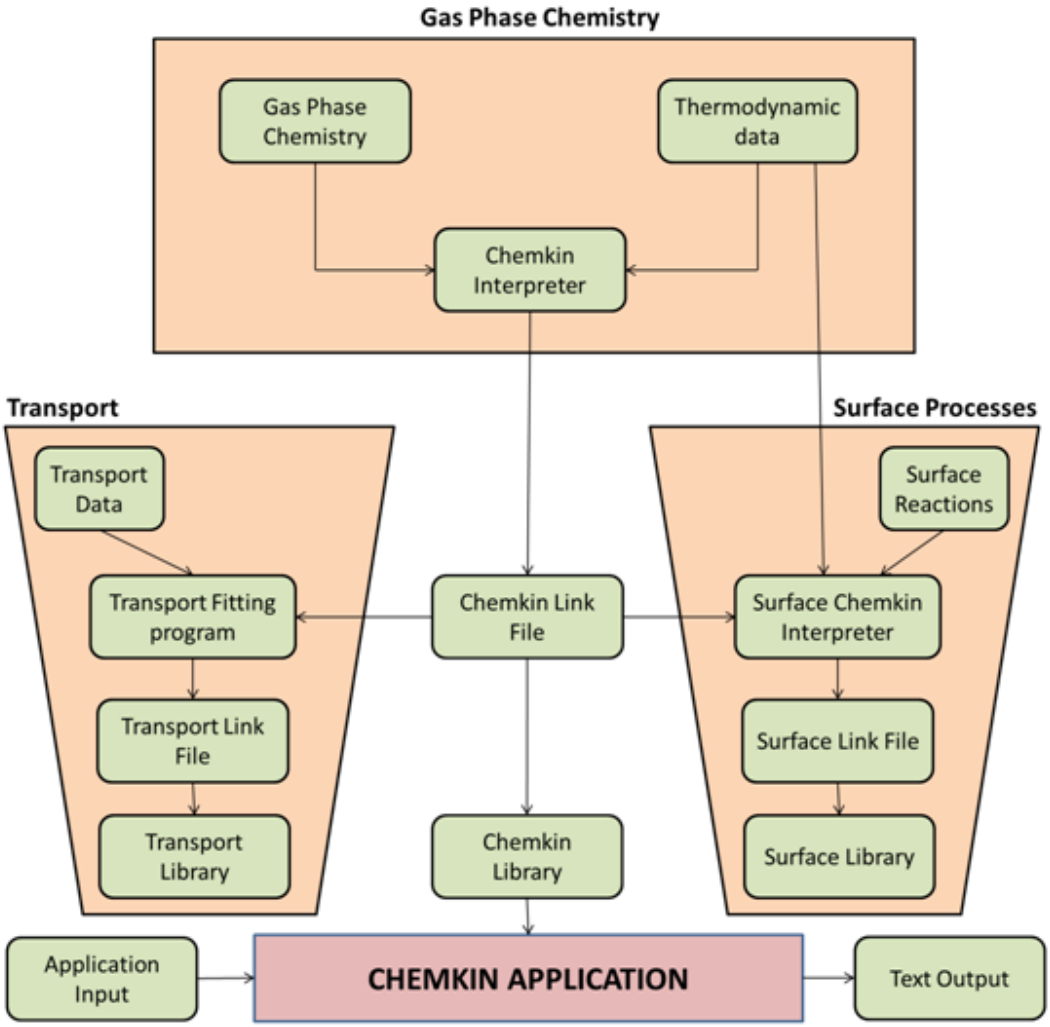

Figure 2-5 The process of CHEMKIN modeling[92]

2.3 CHEMKIN modeling

Until now, there are a lot of softwares developed for combustion modeling and kinetics study. CHEMKIN[93] is designed for modeling various chemical reacting flow configurations and combustion conditions. The gas phase kinetics, surface phase kinetics, equilibrium and transport properties can be defined in the CHEMKIN software to construct models.

CHEMKIN can solve various types of problems, including calculation of adiabatic flame temperatures, equilibrium concentrations for gas mixtures, reactor kinetics, flame speed, species mole fractions and temperature profiles, etc. Using CHEMKIN, it is flexible in choosing the involved species and reactions in analyzing mechanisms. The input files must be written in a typical standardized format specified by CHEMKIN.

The process to develop a CHEMKIN application is shown in Figure 2-5[92].

a) To solve a problem using CHEMKIN, the beginning step is to create an input file which specifies the involved elements and species. The input file should include the thermodynamic data, which includes the curve fit coefficient for calculation of enthalpy and specific heats, as well as the transport data. The details about the chemical reactions and the Arrhenius parameters are also necessary.

b) Creating the make files is the next step. The makes files play a role on linking the libraries of CHEMKIN and then an executable file is form. After that it returns back to comprise of core libraries and convert the text input file into a binary file. After the formation of binary file and the initialization, it is necessary to create another make file which links the application codes, serving specific purposes, to the core libraries.

Chapter 3
Simulation of Hydrogen Enriched Natural Gas Combustion in a Channel Reactor

3.1 Introduction

In this chapter, the hydrogen enriched natural gas combustion in a channel reactor would be numerically studied. Through the simulation results, the hydrogen and catalysts effects on natural gas combustion would be analyzed as well as other parameters, such as temperature and flow rate.

3.2 Numerical Setup

3.2.1 Problem description

The considered rectangular channel is shown in Figure 3-1. It consists of two parallel Pt-coated walls that are h= 7 mm apart and L= 40 cm long. A pre-heated fuel/air mixture composed of CH_4, H_2, O_2, and N_2 enters the channel from the left end at a temperature T_m= 500 K and a uniform velocity u_m=2 m/s. The temperature of the walls, T_w, and the pressure throughout the channel, p, are taken to be uniform and set to be 1200 K and 1 atm, respectively.

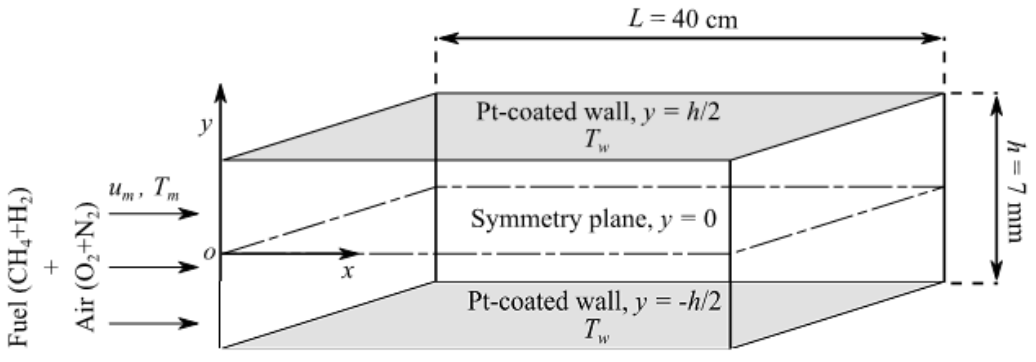

Figure 3-1 Scheme of reactor geometry

Four fuel/air mixtures are investigated. The compositions are provided in Table 3-1. The fuel in mixture 1 is pure CH_4, whereas mixtures 2-4 contain increasing levels of H_2 additives. The mole fractions of CH_4 and H_2 in these mixtures are adjusted such that the mole fractions O_2 and N_2 mole remain unchanged from mixture 1. By virtue of symmetry, the computational domain consists of the upper half of the channel.

Table 3-1 Fuel and air compositions in molar fractions

case	H_2	CH_4	O_2	N_2	H_2/Fuel[a]	Fuel/Air[b]
1	0.00	0.048	0.2	0.752	0.00	0.05
2	0.0024	0.0456	0.2	0.752	0.05	0.05
3	0.0048	0.0432	0.2	0.752	0.10	0.05
4	0.0072	0.0408	0.2	0.752	0.15	0.05

[a, b] These ratios are calculated by volume

3.2.2 Governing equations

The planar channel shear-layer flow reactor model of CHEMKIN[94] is employed to perform the calculations. The model applies the Von Mises transformation to express the boundary-layer equations in terms of the streamwise (axial) coordinate x and the normalized stream function ξ, which is defined as:

$$\xi = \frac{\Psi}{\dot{m}} \qquad \textbf{(3-1)}$$

$\dot{m}$: local total mass flux;

ψ: stream function.

$$\Psi = \int_0^y \rho u dy \qquad \textbf{(3-2)}$$

ρ: density;

u: velocity;

y: cross-stream (transverse) coordinate.

Momentum equation

The momentum conservation equation reads:

$$\rho u \frac{\partial u}{\partial x} - \frac{\rho u}{\dot{m}}\left(\xi \frac{d\dot{m}}{dx} - \frac{d\dot{m}_c}{dx}\right)\frac{\partial u}{\partial \xi} + \frac{dP}{dx} = \frac{\rho u}{\dot{m}^2}\frac{\partial}{\partial \xi}\left(\rho u \mu \frac{\partial u}{\partial \xi}\right) \quad \textbf{(3-3)}$$

$\dot{m}_c$:mass flux at the centerline;

p: pressure;

μ: viscosity.

Energy equation

$$\rho u c_p \frac{\partial T}{\partial x} - \frac{\rho u c_p}{\dot{m}}\left(\xi \frac{d\dot{m}}{dx} - \frac{d\dot{m}_c}{dx}\right)\frac{\partial T}{\partial \xi} =$$

$$\frac{\rho u}{\dot{m}^2}\frac{\partial}{\partial x}\left(\rho u \lambda \frac{\partial T}{\partial \xi}\right) - \sum_{k=1}^{K_g} \dot{\omega}_k W_k h_k - \frac{\rho^2 u}{\dot{m}} \sum_{k=1}^{K_g} Y_k V_{k,y} c_{Pk} \frac{\partial T}{\partial \xi} \quad \textbf{(3-4)}$$

T: temperature;

$c_{p:}$ specific heat;

λ: thermal conductivity;

W_k: molecular weight;

$h_{k:}$enthalpy of species k;

$c_{pk:}$ specific heat of species k.

The effect of radiative heat transfer is neglected in Eq. (3-4) based on the findings of Mazumder and Grimm [95].

Gas Phase species equation

$$\rho u \frac{\partial Y_k}{\partial x} - \frac{\rho u}{\dot{m}}\left(\xi \frac{d\dot{m}}{dx} - \frac{d\dot{m}_c}{dx}\right)\frac{\partial Y_k}{\partial \xi} = \dot{\omega}_k W_k - \frac{\rho u}{\dot{m}}\frac{\partial}{\partial \xi}\left(\rho Y_k V_{k,y}\right)$$

$$k = 1, \dots, K_g \quad \textbf{(3-5)}$$

$Y_{k:}$mass fraction;

$\omega_{k:}$ net chemical reaction rate;

W_k: molecular weight;

$V_{k,y}$: diffusion velocity of species k;

K_g: number of the gas-phase species.

Surface species coverage equation

The steady-state surface species coverage equation is given by:

$$\dot{s}_{k,m} = 0, k = K_s^f(n,m), \dots, K_s^l(n,m) - 1; n = N_s^f(m), \dots, N_s^l(m)$$

$$m = 1, \dots, M \qquad \textbf{(3-6)}$$

$s_{k,m}$: molar production rate of the k^{th} surface species due to surface reactions on material m;

$N_s(m)$: number of surface phases on the m^{th} material;

$K_s(n,m)$: number of surface species for surface phase number n on the m^{th} material;

The superscripts "f" and "l" denote first and last, respectively.

Equation 3-6 is solved subject to the requirement

$$\sum_{k=K_s^f(n,m)}^{k=K_s^l(n,m)} Z_k(n) = 1 \qquad \textbf{(3-7)}$$

$Z_k(n)$: site fraction or site coverage of species k on site n.

The surface molar concentration of species k is obtained from

$$[X_k] = Z_k(n)\frac{\Gamma_n}{\sigma_k(n)} \qquad \textbf{(3-8)}$$

Γ_n: surface site density, assumed to be constant and set to 2.72×10^{-9}mol/cm^2;

$\sigma_k(n)$: number of sites that species k occupies;

M_s: total number of surface species.

Total mass flux

The total mass flux, $\dot{m}$, is calculated through the solution of the equation

$$\frac{d\dot{m}}{dx} = \frac{d\dot{m}_c}{dx} + \frac{d\dot{m}_w}{dx},\ \frac{d\dot{m}_c}{dx} = \rho v|_{y=0};\quad \frac{d\dot{m}_w}{dx} = -\rho v|_{y=h/2} \qquad \textbf{(3-9)}$$

m_c: mass fluxes at the centerline;

m_w: mass fluxes at the wall (upper boundary).

The transverse velocity component v is evaluated from:

$$v = \frac{1}{\rho}\sum_{m=1}^{M}\sum_{k=1}^{K_g}\dot{s}_{k,m}W_k a_m \qquad \textbf{(3-10)}$$

a_m: surface area fraction of the m^{th} material on the wall.

Pressure

The pressure is computed using the ideal gas equation of state

$$p = \frac{\rho RT}{\bar{W}} \qquad \textbf{(3-11)}$$

R: ideal gas constant;

$\bar{W} = [\sum_{k=1}^{K_g} {Y_k}/{W_k}]^{-1}$: mean molecular weight.

Diffusion velocity

Assuming mixture-averaged transport properties, the diffusion velocity is obtained from

$$V_{k,y} = -\frac{D_{km}\rho u}{X_k \dot{m}}\frac{\partial X_k}{\partial \xi} - \frac{D_k^T}{\rho Y_k}\frac{\rho u}{T\dot{m}}\frac{\partial T}{\partial \xi} \qquad \textbf{(3-12)}$$

X_k:molefractionof species k;

D_{km}: mixture diffusion coefficientof species k;

D_k^T: thermal diffusion coefficient of species k.

Transport properties

The coefficients D_{km} are evaluated using:

$$\boldsymbol{D_{km} = (\sum_{\substack{j=1 \\ j\neq k}}^{K_g} W_j D_{k,j} \frac{\partial X_j}{\partial \xi})(\overline{W} \sum_{\substack{j=1 \\ j\neq k}}^{K_g} \frac{\partial X_j}{\partial \xi})^{-1}} \quad \textbf{(3-13)}$$

$D_{k,j}$: multi-component diffusion coefficient matrix.

The coefficients D_k^T are computed by solving a system of equations involving the coefficientsD_{jk} ,X_k, and the thermodynamic and molecular properties of the species. Further details are available in[94]. The mixture-averaged thermal conductivity and viscosity are calculated from:

$$\boldsymbol{\lambda = \frac{1}{2}[\sum_{k=1}^{K_g} X_k \lambda_k + \left(\sum_{k=1}^{K_g} \frac{X_k}{\lambda_k}\right)^{-1}]} \quad \textbf{(3-14)}$$

$$\boldsymbol{\mu = \sum_{k=1}^{K_g} \frac{X_k \mu_k}{\sum_{j=1}^{K_g} X_j \phi_{kj}}} \quad \textbf{(3-15)}$$

$$\boldsymbol{\phi_{kj} = \frac{1}{\sqrt{8}}(1 + \frac{W_k}{W_j})^{-1/2}[1 + \left(\frac{\mu_k}{\mu_j}\right)^{\frac{1}{2}} \left(\frac{W_k}{W_j}\right)^{\frac{1}{4}}]^2} \quad \textbf{(3-16)}$$

λ_k:thermal conductivity of species k;

μ_k: viscosity of species k.

The details concerning the evaluation of these two quantities can be found[94].

3.2.3 Boundary conditions

Constant-velocity boundary conditions are set at the inlet and the species mole fractions of the fuel/air mixture are specified following Table 3-1. Constant-temperature and no-slip boundary conditions are employed at the upper wall. The surface species boundary conditions in CHEMKIN are set by balancing the convective and diffusive mass fluxes of the gas-phase species by the production rates of gas-phase species due to surface reactions:

$$\rho Y_k(v + V_{k,y}) = \sum_{m=1}^{M} W_k a_m \dot{s}_{k,m}\,, k = 1, \ldots, K_g \qquad \textbf{(3-17)}$$

3.2.4 Numerical details

The governing equations in CHEMKIN are discretized using the finite difference method. All first and second derivatives are approximated by central differences. The employed mesh consists of 400 uniformly-distributed grid points in the axial direction and 200 unevenly-spaced points in the transverse direction.

The grid density in the latter direction is highest near the wall to resolve the details of the boundary layer and decreases progressively towards the center line. Several tests were performed to ensure that the selected resolution guarantees grid independent results. CHEMKIN employs the differential/algebraic equation solver DASSL [96] for the solution of the system of equations. The absolute and relative solver tolerances are set to 10^{-12} and 10^{-6}, respectively.

3.2.5 Chemical kinetics

Unless indicated, the calculations employ the gas-phase chemical kinetics mechanism GRI-Mech 3.0 [30] in conjunction with the heterogeneous surface reaction mechanism of Deutschmann et al. [8]. GRI-Mech3.0 is optimized for the combustion of CH_4 and natural gas over a wide range of operating conditions. It consists of 325 elementary chemical reactions involving 53 species including NO_x chemistry. The mechanism of Deutschmann et al. drives the kinetics of H_2-assisted catalytic combustion of CH_4 on Pt. It includes 24 reactions and 11 surface species, namely H(S), O(S), OH(S), H_2O(S), C(S), CO(S), CO_2(S), CH_3(S), CH_2(S), CH(S), and Pt(S).

3.3 Results and discussion

3.3.1 Effect of H2 additives

The effect of H_2 additives on the combustion of CH_4 is investigated. Two sets of calculations are performed for every mixture in Table 3-1. The first set does not involve a catalyst at the wall, whereas Pt-catalyst is included in the second. As such, the first set serves as a benchmark against which the impact of catalytic reactions on combustion is evaluated.

3.3.1.1 Non-catalytic combustion

Figure 3-2shows the profiles of the mean axial temperature obtained from the non-catalytic calculations. As the H_2 content in the fuel is increased, the temperature profiles reach their peaks closer to the inlet, indicating shorter preheating distances and ignition delays during the transient period preceding the ignited steady-state. Further, increasing the levels of H_2 leads to lower ignition temperatures. The peak temperature decreases from 1900 to 1450 K when the H_2 content is increased from 0 (mixture 1) to 15% (mixture 4). The trends observed in Figure 3-2are attributed to the lower ignition temperature of H_2 compared to CH_4. Accordingly, increasing the H_2 content in the fuel leads to faster ignition as the heat released by the H_2 oxidation reactions promotes the ignition of CH_4. Upon ignition, the thermal fluxes out of the ignition zone lead to the upstream propagation of burnt products species towards the unburnt (cold) fuel/air mixture incoming from the inlet. Since ignition takes place closer to the inlet with increasing H_2 content, a wider section of the channel becomes reacted.

Beside the temperature, the history of OH evolution is often employed as a numerical tool for the determination of the location and time of ignition in transient simulations due to its luminous properties. The analysis of the trends of the mean OH mole fractions trends, which are displayed in Figure 3-3, remains useful for the understanding of the ignited steady-state. As the H_2 content is increased, OH exhibits a sudden increase closer to the inlet of the channel at the same axial locations where the temperature peaks abruptly upon mixture preheating in Figure 3-3. This trend confirms the conclusions drawn from the latter figure in regards to the effect of H2 on the length of preheating distances and ignition delays. The

magnitudes of the OH peaks depend on the H_2-to-fuel ratios and the reaction temperature. For high ratios, the reaction temperature is lower, and therefore, the peaks are smaller. It is worth noting that that two OH peaks manifest in mixtures 3 (10% H_2) and 4 (15% H_2) compared to one peak in mixtures 1 (0% H_2) and 2 (5% H_2). Increased H_2 levels in the fuel result in two instances of ignition. Due to its lower ignition temperature, H_2 ignites first leading to the first OH peak. The heat release associated with this ignition event triggers the ignition of CH_4, which results in the second OH peak. The occurrence of two ignition events explains the finite slope ahead of the peaks of the temperature profiles of mixtures 3 and 4 in Figure 3-2. In these two mixtures, the initial temperature increase occurring after preheating is sharp. Then the temperature continues to increase but at slower rate. On the other hand, the slope of the temperature in mixtures 1 and 2 is nearly infinite due to the occurrence of single ignition event.

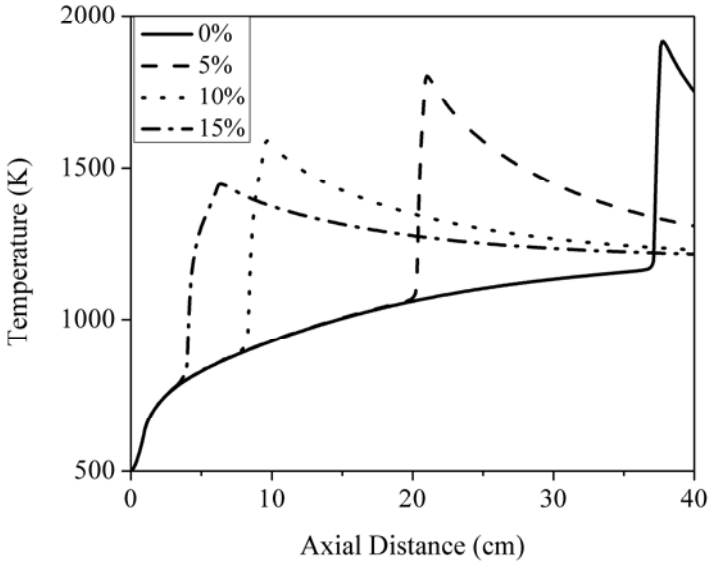

Figure 3-2 Effect of H_2 additives in the absence of Pt catalyst: mean axial temperature

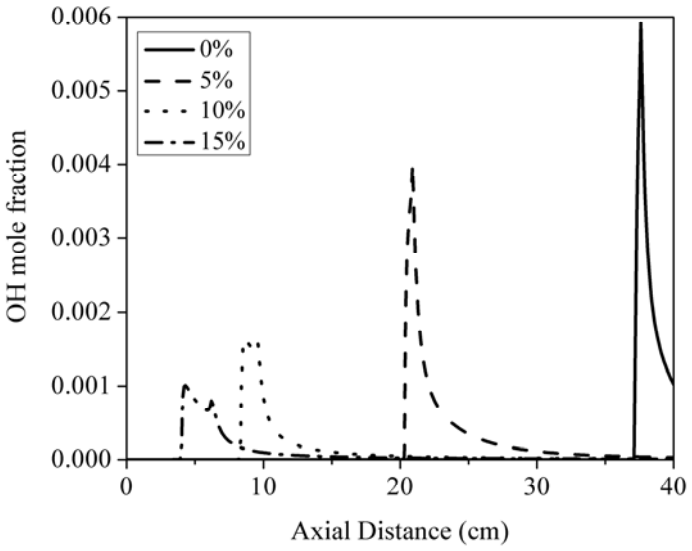

Figure 3-3 Effect of H_2 additives in the absence of Pt catalyst: mean axial OH mole fraction

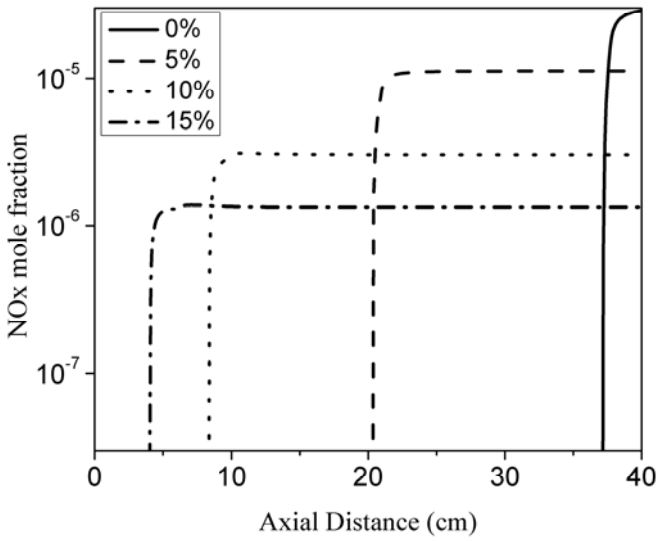

Figure 3-4 Effect of H_2 additives in the absence of Pt catalyst: mean axialNO mole fraction

Figure 3-4 shows the axial variation of the mean NO_x mole fractions. As the H_2 content is increased, NO_x levels decrease due to the decrease in to the lower mean axial temperatures (Figure 3-2). In all 5 mixtures, NO_x emerges when the mixture ignites. The formation of NO_x is temperature dependent. It takes place through thermal pathway at high temperatures and through prompt pathway at lower temperatures. Figure 3-4 reveals that NO_x is predominantly produced via the former pathway since the mean temperature is sufficiently high. Therefore, the trends of the NO_x profiles align with those of the temperature.

3.3.1.2 Catalytic combustion

Apart from the inclusion of Pt-catalyst at the wall, the operating conditions T_w, T_m, u_m and P in the following set of calculations are unchanged from the previous set. The aim is to determine the effect of catalysis on the combustion of the same mixtures investigated in the previous section. Figure 3-5 displays the variation of the mean axial temperature. Increasing the H_2 content in the fuel enhances the preheating of the mixture and results in a decrease in the peak temperature. In contrast to the non-catalytic realizations (Figure 3-2), the temperature in all mixtures does not exhibit an abrupt increase, which indicates that the ignited steady-state does not involve any ignition events. The trends of the temperature profiles in Figure 3-5 suggest the structure of a propagating premixed flame. The temperature increases gradually from the inlet then peaks in the Reaction Zone (RZ) around two-thirds of the channel length before decaying slowly in the post flame zone as the burnt mixture approaches the outlet. The decay of the temperature in downstream locations is attributed to the fact that $T_w$is lower than the temperatures attained in the RZ. Therefore, the H_2-assisted catalytic combustion of CH_4 enhances the stability of burning in the channel, consistent with the findings of Zhang et al. [97]. Compared to the non-catalytic cases, the axial locations of the peaks in all mixtures do not show appreciable differences. Further, although the magnitudes of the peaks dampen with increasing H_2 content, the overall mean channel temperature is significantly lower in all mixtures, and H_2 seems to have a less important but non-negligible effect on heat release.

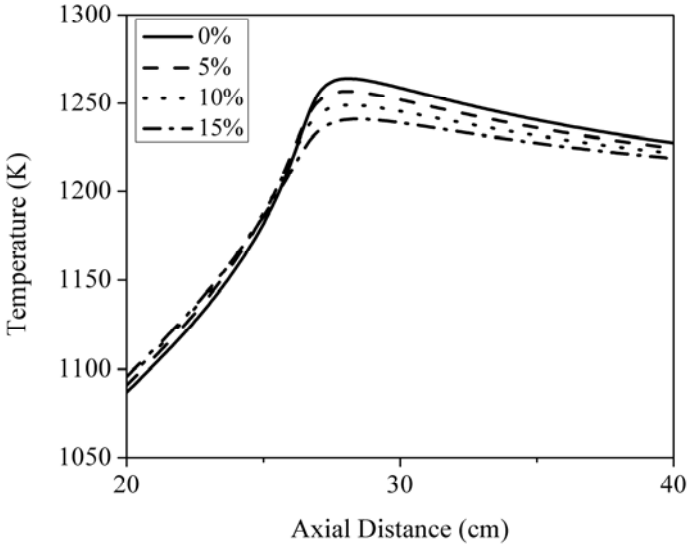

Figure 3-5 Effect of H_2 additives in the presence of Pt catalyst: mean axial temperature

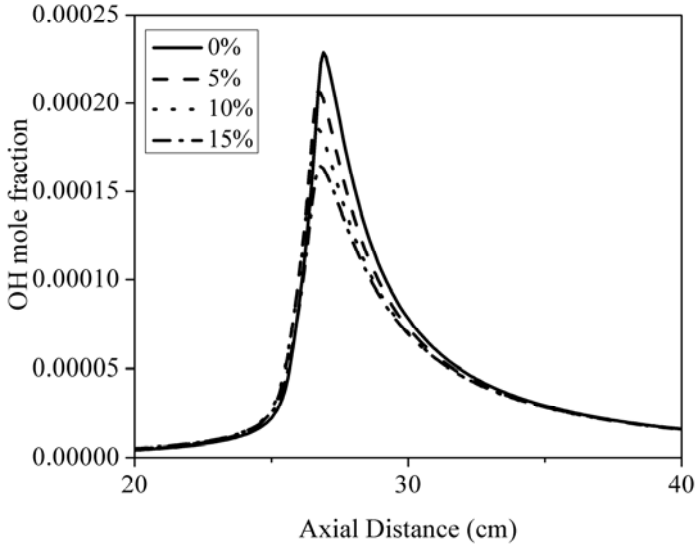

Figure 3-6 Effect of H_2 additives in the presence of Pt catalyst: mean axial OH mole fraction

Compared to the non-catalytic case, the mean axial OH profiles in the catalytic realization shown in Figure 3-6 achieve their maxima in the RZ and their peak values are one order of magnitude lower. The absence of spikes from the profiles indicates that the ignited steady-state does not involve ignition events, which confirms the conclusion drawn previously from temperature profile.

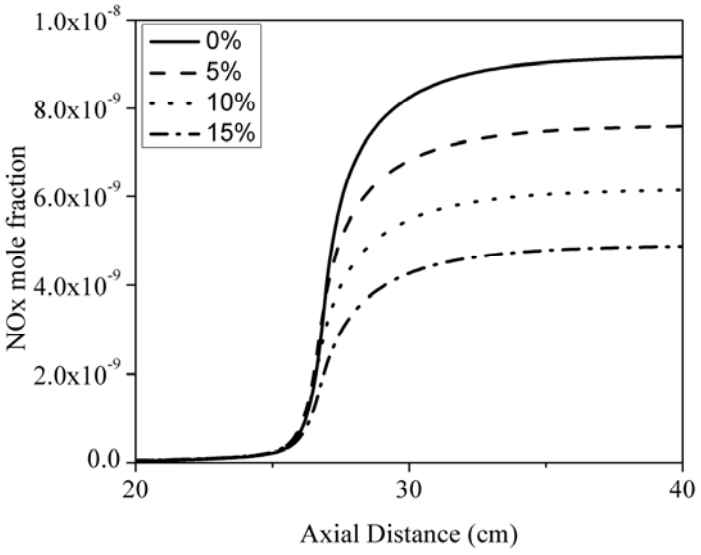

Figure 3-7 Effect of H_2 additives in the presence of Pt catalyst: mean axial NO mole fraction

Figure 3-7 displays the mean axial NOx profiles. NO_x emissions decrease with increasing H_2 content by virtue of the lower reaction temperature. Compared to the non-catalytic results presented earlier in Figure 3-4, the levels of NO_x in all mixtures are several orders of magnitude lower. This reduction is attributed to the lower reaction temperatures (compare Figure 3-5 to Figure 3-2). Table 3-2 provides the predicted mean NO_x mole fractions at the channel outlet for all mixtures in the non-catalytic and catalytic realizations. In both cases, NO_x levels decay with increasing H2 content. When H2 is added to the fuel, less CH_4 becomes available for reaction. Therefore, lower NO_x emissions are obtained at the outlet

since the oxidation of CH_4 is the primary NO_x contributor. It is clear for all mixtures that surface reactions lead to significantly lower NO_x levels. The formation NO_x in the non-catalytic calculations was deemed to occur mainly through thermal pathways at high temperatures. Here, however, the substantially lower emission levels at reduced reaction temperatures suggest that NO_x forms through prompt pathway.

Table 3-2 Predicted mean NO_x mole fractions (ppm) at the channel outlet in the non-catalytic and catalytic reactions

Mixture	1	2	3	4
Without Pt	28.3	11.2	3.0	1.3
With Pt	0.009	0.007	0.006	0.005

The stream wise surface coverage values of selected surface species are plotted in Figure 3-8. Only the results of mixtures 1 (0% H_2) and 4 (15% H_2) are shown. In both mixtures, the surface coverage of O(S) and Pt(S) are substantially higher than the surface coverage of the remaining surface species. Therefore, the catalytic surface is mainly covered by Pt(S) and O(S), which is the case in fuel-lean combustion. The adsorption of oxygen is more likely to occur at lower temperatures due to its higher sticking coefficient on the Pt surface. The coverage of O(S) is primarily controlled by the temperature distribution in the channel due to the dependence of its adsorption rate on the temperature. The O(S) coverage reaches its lowest level where the temperature is the highest (x= 27 cm). The coverage of H(S) is mainly controlled by the near-wall concentration of H_2 and the adsorption rate of H2 is at the first order with respect to Pt. Therefore, the coverage of H(S) varies from mixture to mixture 4since the two mixtures differ in their initial H_2 content. However, since the change in PT(S) coverage is minimal, the adsorption rate of H_2 does not change significantly. As such, the levels of H(S) in the two cases show marginal differences. The surface coverage of CO(S) and CO2(S) decays sharply beyond the RZ, indicating that carbon species on the catalytic surface are reduced by continuous surface reactions with the gas phase species.

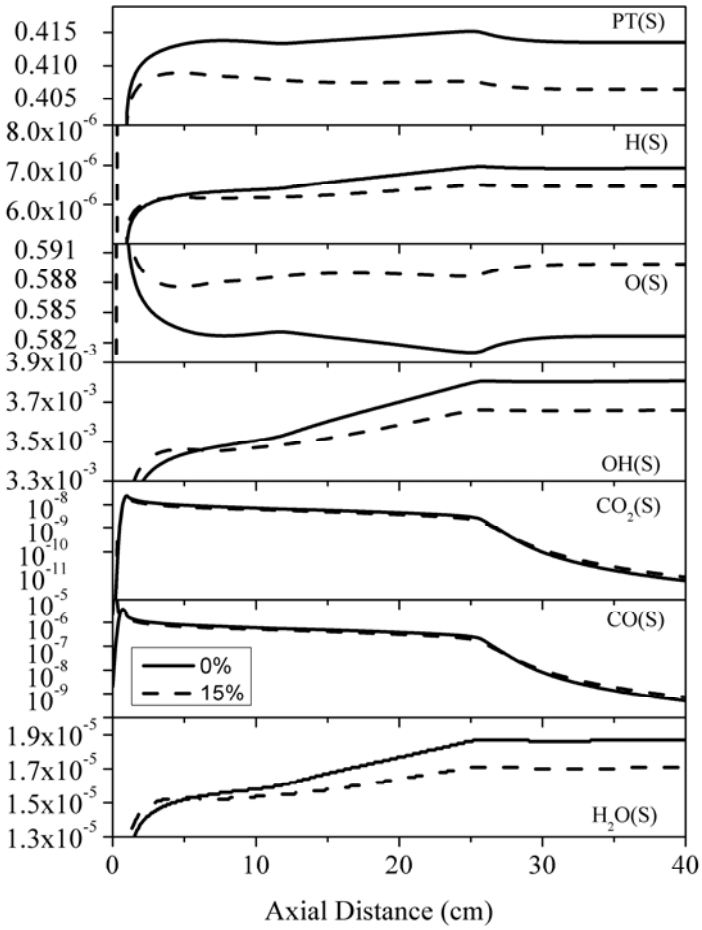

Figure 3-8 Effect of H_2 additives in the presence of Pt catalyst: streamwise surface coverage for mixtures 1 (0%H_2) and 4 (15% H_2).

3.3.2 Effect of operating conditions

In the previous section, it was shown that H_2 additives have a significant effect on the catalytic and non-catalytic combustion of CH_4. In addition to the composition of the fuel/air mixture, other operating conditions, such as T_m and T_w can influence the combustion process. In this section, the impact of these two parameters is investigated by varying them

independently. Calculations are performed for mixture 4 (15%H_2) in the presence of Pt-catalyst.

3.3.2.1 Impact of fuel/air mixture temperature

Three fuel/air mixture temperatures are considered, namely T_m= 400, 500, and 600 K. T_w is held constant at 1200 K. The mean axial OH mole fractions are shown in Figure 3-9. As expected, when Tm is increased the preheating distance decreases and the RZ shifts to upstream locations. The higher OH levels in the RZ are attributed to the increased mean axial temperature.

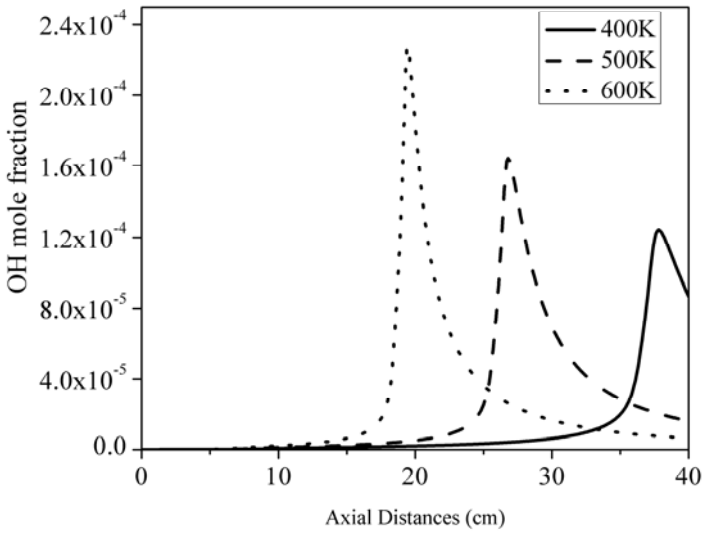

Figure 3-9 Effect of fuel temperature: mean axial OH mole fraction

The streamwise surface coverage of selected surface species is displayed in Figure 3-10 for T_m= 400 and 600 K. As in the previous section, the catalytic surface using both mixture temperatures is mostly covered by Pt(S) and O(S). The variations of the coverage of H(S) and H_2O(S) are small throughout the channel. The differences in the coverage of CO(S) and CO_2 (S) are negligible in the preheat zone and become more substantial beyond the RZ.

When T_m= 600 K, The lower levels of these two surface species downstream of the RZ are attributed to the higher mean temperature and gaseous CO and CO_2 values.

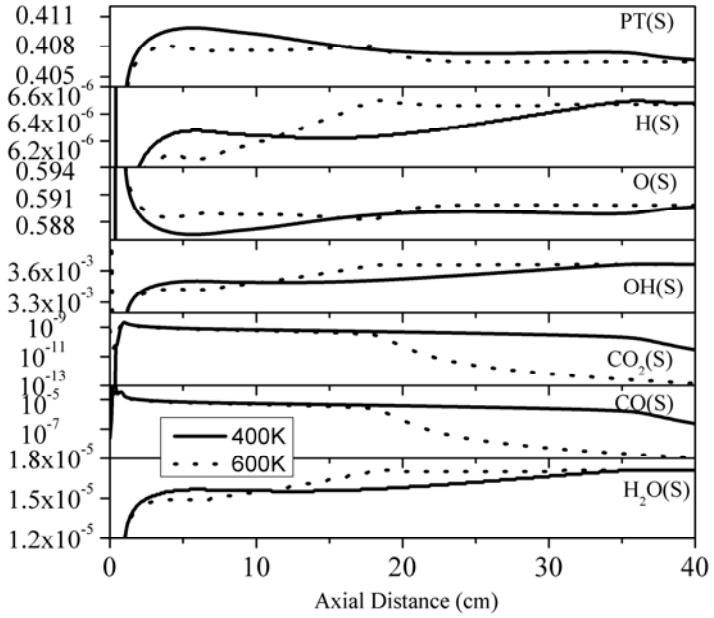

Figure 3-10 Effect of fuel temperature: streamwise surface coverage for T_m = 400 K and 600 K. All calculation employ T_w = 1200 K

3.3.2.2 Impact of wall temperature

Since T_w is maintained constant throughout this work, the investigation of the effect of this parameter on the behavior of the fuel/air mixture is essential. Three wall temperatures are examined, T_w= 1000, 1200, and 1400 K, whereas T_m is kept constant at 500 K. When T_w= 1000 K, the mixture remains nearly inert, with little signs of reactions. This can be clearly seen from the negligible yet increasing mean OH mole fractions in Figure 3-11.

As T_w is increased the mixture reacts. However, the dynamics of reaction depend on the magnitude of T_w. When T_w= 1200 K, no ignition events are observed in steady-state, as described in section 3.3.1.2. By increasing T_m further to 1400 K, two ignition events occur

upstream of the entrance of the channel. This can be seen from sudden increase in OH aroundx≈2.5 cm, which corresponds to the ignition of H_2, and from the peak located at x≈8 cm, which is associated with the ignition of CH_4. Therefore, large T_w has a destabilizing effect on catalytic combustion. The observed variability in the responses of the mixture indicates that the extent of stability offered by catalytic surface reactions is prone to T_w.

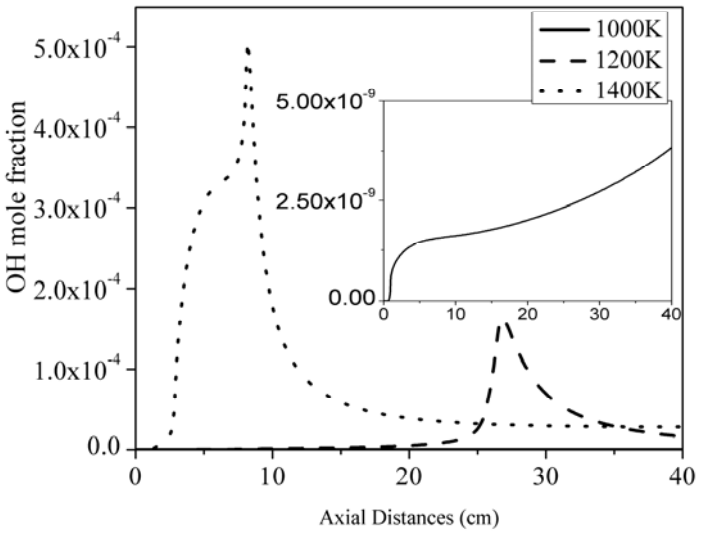

Figure 3-11 Effect of wall temperature: mean axial OH mole fraction

Figure 3-12 displays the streamwise surface coverage of selected surface species for T_w= 1000 and 1400K. Only the results of mixtures 1 (0% H_2) and 4 (15% H_2) are shown. In both mixtures, the surface coverage of O(S) and Pt(S) are substantially higher than other surface species. Thus, the catalytic surface is mainly covered by O(S) and Pt(S), as mentioned before. The coverage of H(S) and H_2O(S) are small all along the channel. But when surface temperature increased, the surface coverage of H(S) would increase a lot, which is caused by the higher Pt(S) coverage. H_2O(S) coverage showed a decrease trend, which results in a higher H_2O content in the gas phase. The difference in the coverage of CO(S) and CO_2(S) are obvious. When T_w=1000K, there is no ignition occurred, CO(S) and CO_2(S) coverage

changes little throughout the whole channel. When T_w=1400K, the gas ignited very fast and the CO(S) and CO2(S) coverage dropped immediately to the gas phase.

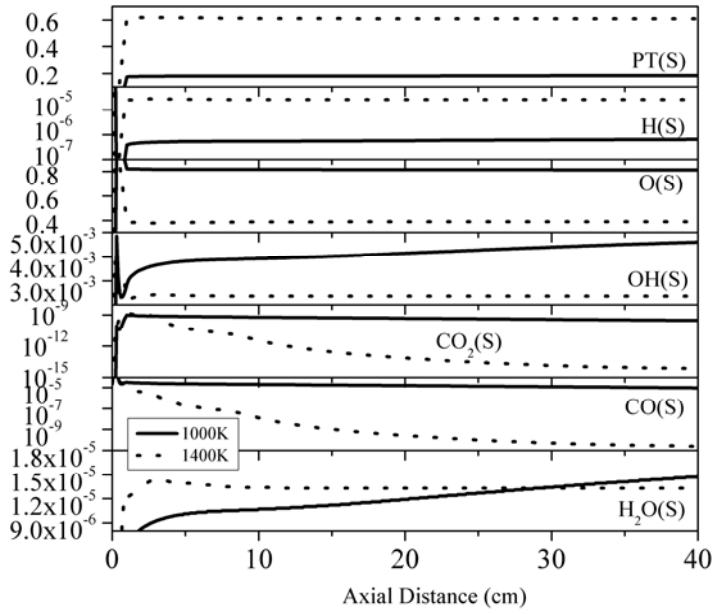

Figure 3-12 Effect of wall temperature: streamwise surface coverage for T_w= 1000 K and 1400 K. All calculation employ T_m = 500 K

3.3.3 Assessment of gas-phase and surface reaction mechanism

Gas-phase and surface reaction mechanisms play a key role in the numerical modeling of reacting flows. To investigate this aspect further, calculations are performed using a number of kinetic schemes. In the following, the composition of mixture 4 (15% H_2) at 500 K is employed at the inlet and the wall temperature is set to 1200 K.

3.3.3.1 Gas-phase mechanism

The considered gas-phase mechanisms are summarized in Table 3-3. GRI-Mech 2.11, GRI-Mech 3.0, and the Miller-Bowman mechanism have comparable numbers of species, with the second being the most detailed in terms of reactions. GRI-Mech 2.11 and GRI-Mech 3.0 cover up to C-2 and C-3 chemistry, respectively, whereas the Miller-Bowman mechanism

includes heavier species, namely C_4H_2 and C_4H_3. In addition to these two species, the relatively less detailed mechanism of Lutz et al. accounts for C_5H_2, C_5H_3, and C_6H_2. The Smooke-Giovangigli mechanism is the least detailed of all schemes, covering only C-1 chemistry. Deutschmann's mechanism is employed throughout this section for the treatment of surface chemistry.

Table 3-3 Gas-phase and surface kinetic mechanisms

Gas-phase chemistry			
Mechanism	Species	Reactions	Ref
GRI-Mech 3.0	53	325	Smith et al.
GRI-Mech 2.11	49	277	Bowman et al.
Miller-Bowman	52	250	Miller and Bowman
Lutz	37	154	Lutz et al.
Smooke-Goivangigli	16	25	Smoke and Giovangigli
Surface chemistry			
Mechanism	Species	Reactions	Ref.
Deutschmann	11	24	Deutschmann et al.
Chou	10	23	Chou et al.

The results obtained using the five gas-phase mechanisms are displayed as following. It is clear that the different kinetic schemes yield substantially different results. As shown in Figure 3-13, when GRI-Mech 3.0 is employed, the mixture exhibits fast preheating and the location of the RZ is farthest from the outlet. The Lutz and Miller-Bowman mechanisms yield virtually identical temperature profiles up to the middle of channel then deviate from one another beyond this point. A RZ develops earlier using the former mechanism, whereas

the mixture continues to preheat using the latter, leading to the development of a RZ farther downstream. When GRI-Mech 2.11 is used, the mixture exhibits nearly inert heating along the channel length and a narrow RZ forms ahead of the outlet. A similar trend is obtained using the Smooke-Giovangigli mechanism; however, preheating occurs at a slower rate and a significantly narrower RZ starts to develop near the outlet of the channel.

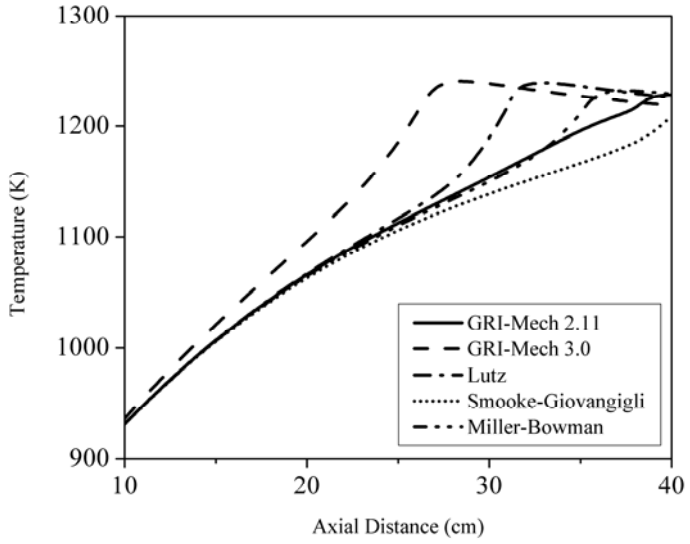

Figure 3-13 Impact of gas phase chemical kinetics on mixture 4 (15%H_2): mean axial temperature

For each mechanism, the mean axial OH mole fractions shown in Figure 3-14 increase slowly in the preheat zone and peak at the axial locations where the RZ develops before decaying towards the outlet. The OH peak resulting from the usage of Lutz mechanism is relatively larger inmagnitude compared to the peaks obtained using GRI-Mech 2.11 and 3.0 and the Miller-Bowman mechanism. This result is associated with the release of H radicals accompanying the formation of C_5H_2, C_5H_3, and C_6H_2 from the reaction between C_4H_2 with the radicals CH, CH_2, and C_2H, respectively. In turn, the increased level of H promotes the formation of OH directly via a number of chain-propagating reactions, and indirectly through the formation of H_2 by means of a number of chain-terminating reactions.

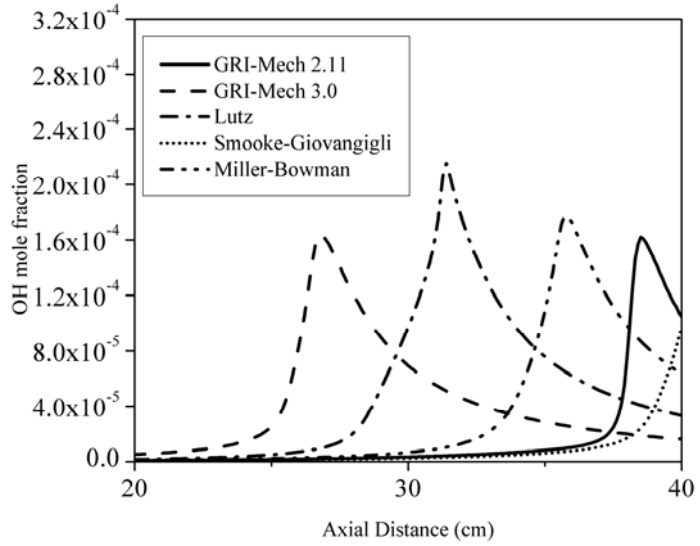

Figure 3-14 Impact of gas phase chemical kinetics on mixture 4 (15%H_2): mean axial OH mole fraction

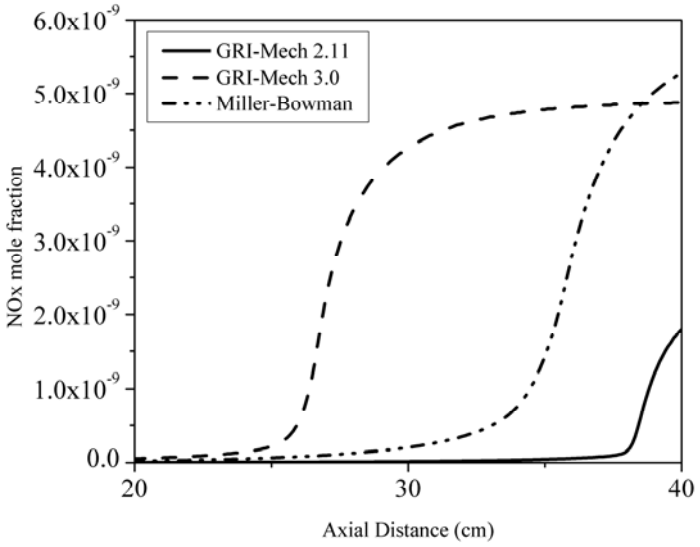

Figure 3-15 Impact of gas phase chemical kinetics on mixture 4 (15%H_2): mean axial NOx mole fraction

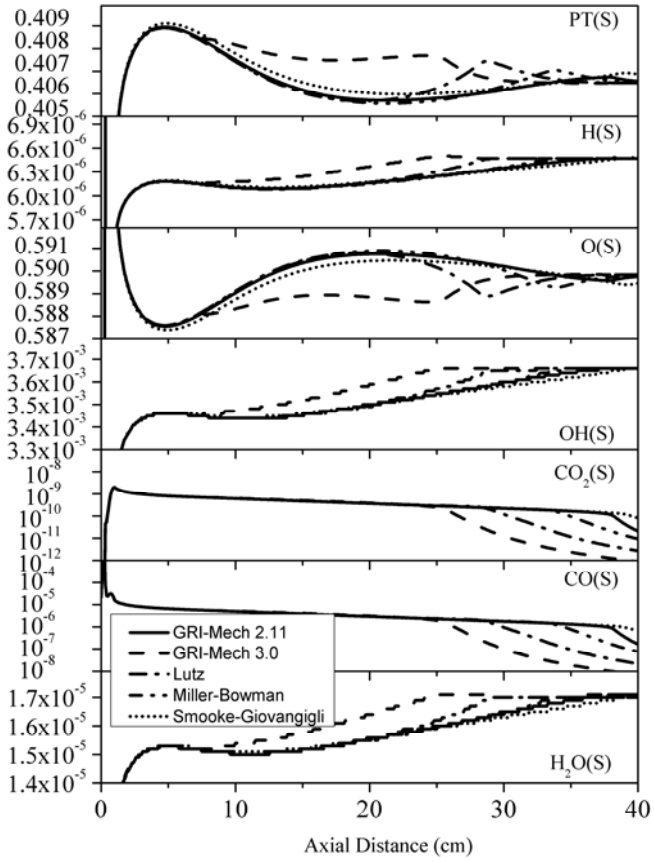

Figure 3-16 Impact of gas phase chemical kinetics on mixture 4 (15%H_2):streamwise surface coverage. All calculation are performed using the Deutschmann mechanism with T_w = 1200 K and T_m = 500 K

The mean axial profiles of NO_x are shown in Figure 3-15. Since the Lutz and Smooke-Giovangigli mechanisms do not account for NO_x chemistry, only the profiles obtained using GRI-Mech 2.11 and 3.0 and the Miller-Bowman mechanism are plotted. As discussed in previous sections, the formation of NO_x is strongly dependent on the temperature. It was previously established using GRI-Mech 3.0 that the overall mean axial temperature decreases

throughout the channel in the presence of Pt-catalyst and as a consequence, NO_x formation occurs mainly through prompt pathways. This conclusion remains unchanged for GRI-Mech 2.11 the Miller-Bowman mechanism. Since preheating is slower when these two mechanisms are employed, the resulting NO_x levels are lower compared to those obtained using GRI-Mech 3.0.

The effects gas-phase kinetics on surface coverage is illustrated in Figure 3-16. The same trends previously described in section 3.3.1.2where GRI-Mech 3.0 is employed are observed here. For all mechanisms, the catalytic surface is mainly covered by Pt(S) and O(S) and the variations of the coverage of H(S) and H_2O(S) are small. Also consistent with previous findings, the differences in the coverage of CO(S) and CO_2(S) prevail beyond the reaction zones where the temperature is high and gaseous CO and CO_2 are abundant. Therefore, gas-phase kinetics mainly affects the coverage of CO(S) and CO2(S). In the absence of experimental measurements, it is difficult to judge which of the gas-phase mechanisms is the most accurate for the considered simulation conditions.

3.3.3.2 Surface mechanism

To further investigate the role of surface chemistry, the performance of the mechanism of Chou et al. is compared previous results obtained using the Deutschmann mechanism. The Chou mechanism involves the same number of surface species and one less reaction. As in the previous section, the composition of mixture 4 is considered with T_m and T_w set to 500 and 1200 K, respectively. The gas-phase kinetics is modeled using GRI-Mech 3.0.

Figure 3-17 displays the mean axial temperature. The trends in both cases are very similar except that preheating occurs at slightly faster rate and the RZ locate further upstream from the outlet when the Chou mechanism is employed. Negligible differences are obtained at downstream axial locations. Since all simulation parameters including gas-phase chemistry are unchanged, the differences observed in Figure 3-17 must originate from the surface chemistry. The Chou mechanism mainly differs from the Deutschmann mechanism by the inclusion of an additional reaction accounting for the adsorption of CH4 in the presence of

O(S) (labeled A3 in Chou's work and referred to as such in the current work) and exclusion of CO_2(S). This adsorption reaction is responsible for the initiation of ignition on surfaces where the coverage of O(S) is high. Since there is no CO_2(S) species in Chou mechanism, the CO_2 releasing process is not a limit step anymore, which will enhance the whole reaction rate. Accordingly, the differences obtained in Figure 3-17 stem from the adsorption reaction A3. During the transient state preceding steady-state, faster ignition is achieved by means of reaction A3. As a result, the steady-state RZ forms at an upstream location in comparison to the Deutschmann mechanism.

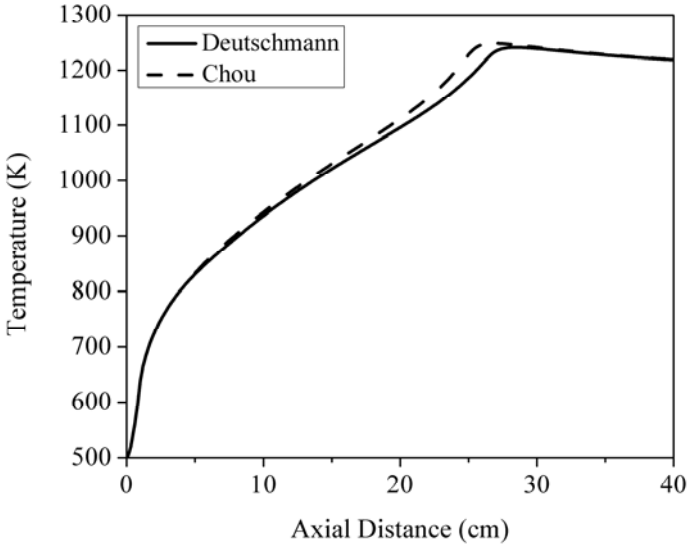

Figure 3-17 Impact of surface chemical kinetics on mixture 4 (15%H_2): mean axial temperature

The mean axial OH mole fractions shown in Figure 3-18 correspond with the temperature profiles shown in Figure 3-17. The OH peak resulting from Chou mechanism is larger compared to the peak obtained using Deutschmann mechanism. As mentioned above, the additional CH_4 adsorption reaction enhances the ignition process and it itself produce OH species. Both of the two effects can results in a higher OH value.

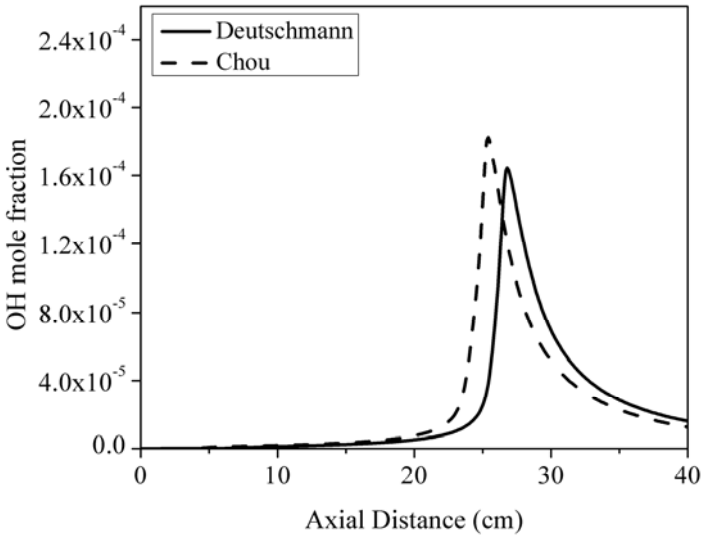

Figure 3-18 Impact of surface chemical kinetics on mixture 4 (15%H_2): mean axial OH mole fraction

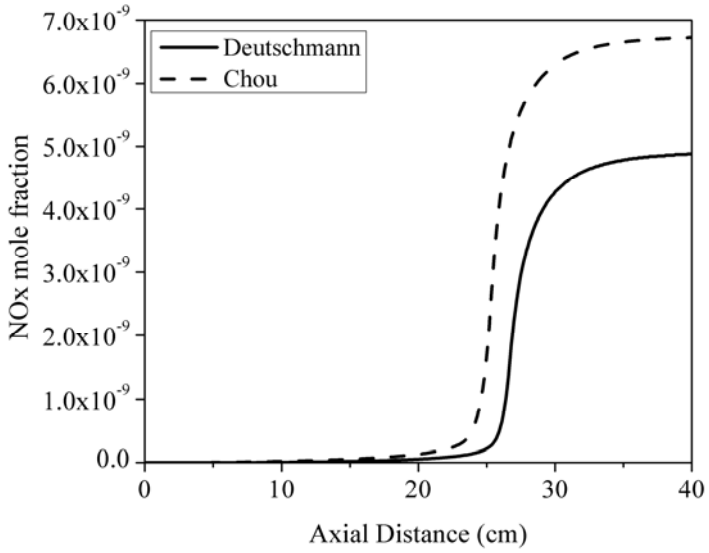

Figure 3-19 Impact of surface chemical kinetics on mixture 4 (15%H_2): mean axial NO_x mole fraction

Figure 3-19 demonstrates the mean axial profiles of NO_x. There are no NO_x species included in the two surface mechanisms, so the NO_x formation is through the gas-phase reactions. As discussed before, temperature is the main factor influencing NO_x formation. Therefore, the NO_xvalues from Chou mechanism are higher than Deutschmann mechanism due to higher reaction temperature.

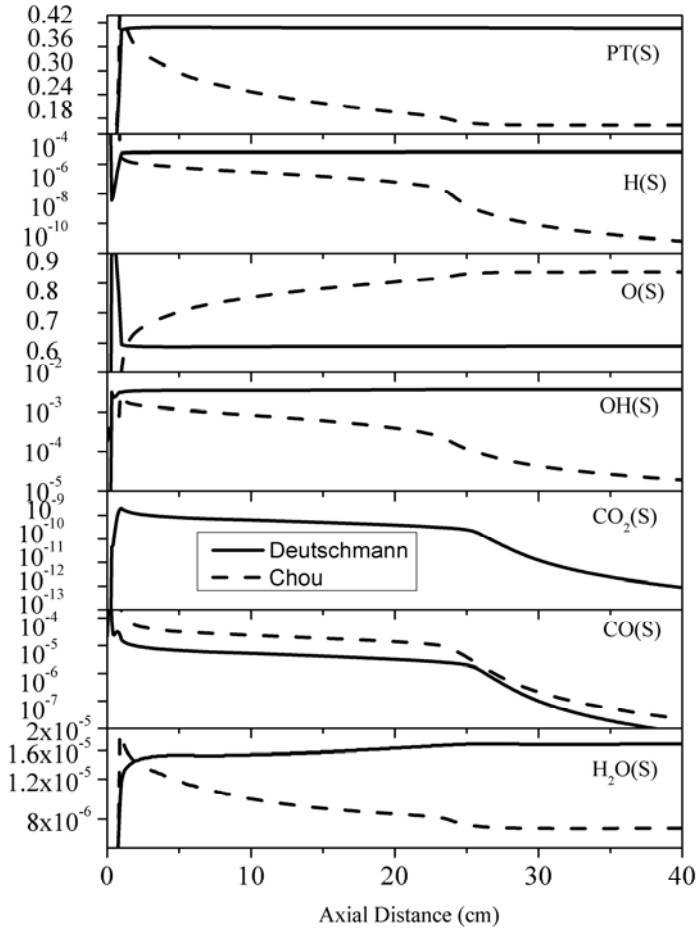

Figure 3-20 Impact of surface chemical kinetics on mixture 4 (15%H2): streamwise surface coverage. All calculation are performed using GRI-Mech 3.0 with T_w = 1200 K and T_m = 500 K

The effects of surface mechanisms on surface coverage are shown in Figure 3-20. As employed different surface kinetics, the surface species coverages change a lot. For the two cases, Pt(S) and O(S) are still dominant species on the catalytic surface. However, in Deutschmann mechanism, Pt(S) and O(S) coverage change little throughout the channel; in Chou mechanism, Pt(S) coverage is decreasing all along the channel and O(S) coverage is increasing all the way. In Chou mechanism, O(S) coverage is much higher than Pt(S) at the end the channel. With the existence of A3, higher level of O(S) will not limit CH4 adsorption, which results in stronger effects of surface mechanism on the whole reaction system. The species of H(S), OH(S), CO(S) and H2O(S) decreased along the channel in the preheating zone and then relatively sharply dropped during RZ.

3.4 Summary

In this chapter, the effects of hydrogen addition and Pt-catalysts on natural gas combustion in a channel reactor are numerically studied. Four gas mixtures are employed in the catalytic and non-catalytic combustion. The influencing factors, including mixture temperature and wall temperature, and different gas and surface mechanisms are investigated.

Hydrogen addition can promote CH_4 ignition significantly and reduce NO formation in the non-catalytic combustion; however, the effects of hydrogen addition to the catalytic combustion are not obvious. Pt-catalyst reduce both the reaction temperature and NO formation a lot. Both higher wall temperature and inlet flow temperature can promote ignition occurring. By employing different mechanism, the obtained ignition and species conditions are very different. However, to determine which mechanism suitable for the actual condition is still remained to be confirmed with experiments.

Chapter 4
Experimental and Numerical Investigation of Natural Gas Combustion on the Counter-Flow Burner

4.1 Introduction

In many combustion studies, the flame must be stable and well-characterized. To get these flames, the counter flow configuration is one of the best methods, by providing simple and stable flame structures. In this chapter, natural gas combustion on the counter flow burner would be investigated in both experimental and numerical methods.

4.2 Experimental setup

The reaction and sampling system was designed and constructed for the methane combustion experiments. The system includes a counter-flow diffusion flame burner, gas supply system, and gas sampling system and gas analyzing device. Figure 4-1 presents a diagram of the system. More details are available in the reference [98].

4.2.1 Counter-flow diffusion flame burner

The counter-flow diffusion flame burner system consists of two opposed burners, which are apart from each other at a distance of 2cm, shown in Figure 4-2. Both of burners contain porous sintered bronze matrix, which can be divided into the inner and outer coaxial cylinders with the diameters of 6.04cm and 7.34mm, respectively. The fuel and oxidizer flows into the reaction zone to form the flame sheet directly from the inner annulus. The protecting gas such as nitrogen or argon can flow through the outer annulus and minimize the disturbance from the surrounding to the flame. In addition, at the center of the bottom burner, there is another port (1/8 inch) which is designed for the addition of catalysts or other additives.

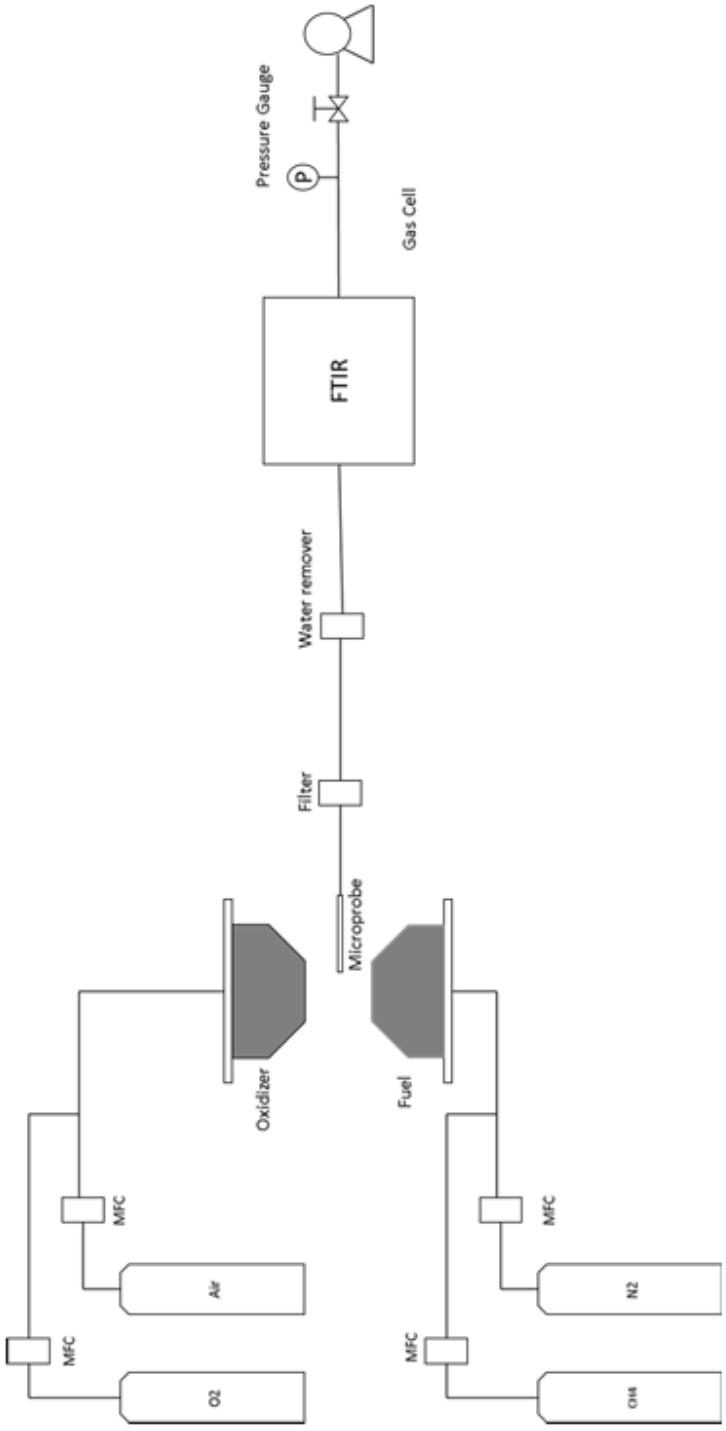

Figure 4-1 Scheme of experimental setup

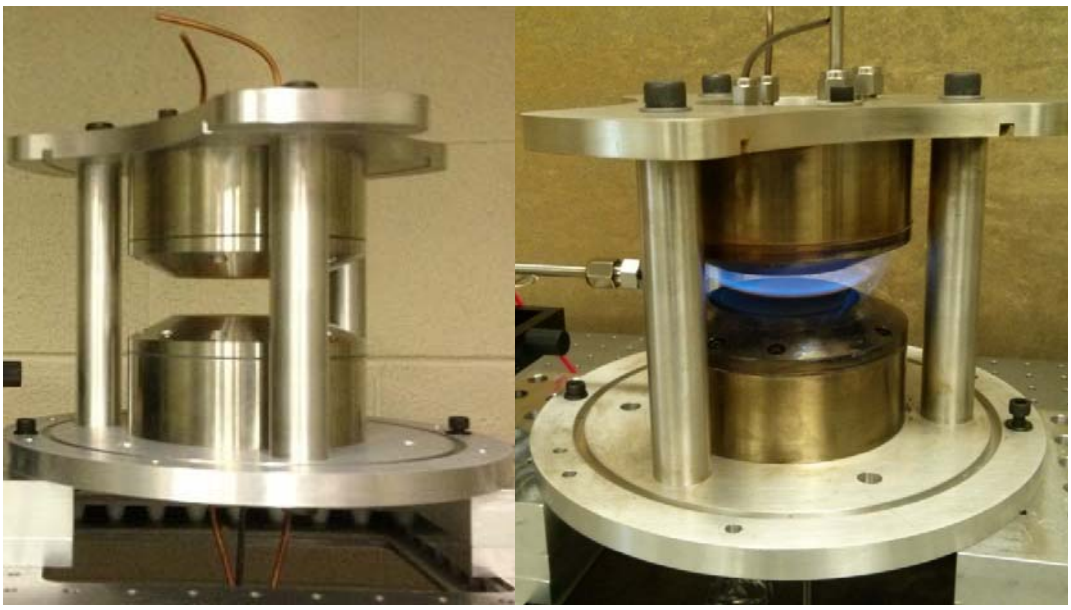

Figure 4-2Structure of counter-flow burner

4.2.2 Gas supply system

In this study, methane mixed with nitrogen is used as fuel, which is fueled from the bottom burner. Air and oxygen is used as oxidizer, which is fueled from the top burner. All the flow rates of the four gases were controlled by mass flow controllers (1% error).

The flow rates are based on the previous study, listed as Table 4-1.

Table 4-1 Flow conditions in the experiments

	Fuel		Oxidizer	
	Methane	Nitrogen	Oxygen	Air
Flow rate (L/min)	1.395	13	3.448	10.242
Mole fraction	0.097	0.903	0.409	0.591
Velocity	8.37		7.96	
Reynold's number	360		342	

To Study different fuel/oxidizer ratios effects on the NO production, two additional methane flow rates (1.8 and 2.2 L/min) are employed. In these two cases, the strain rates, which can be calculated as Equation 4-1, are kept consistent with the first case, 16.7s^{-1}; the flow rates of oxidizer (oxygen and air) are kept the same condition as Table 4-1 lists. N_2 flow rates are adjusted to balance the strain rates.

$$\mathbf{a = 2\frac{|U_{fuel}|}{L}\left(1+\frac{|U_{oxidizer}|\sqrt{\rho_{oxidizer}}}{|U_{fuel}|\sqrt{\rho_{fuel}}}\right)} \qquad \textbf{(4-1)}$$

a: strain rate of the fuel side (s^{-1});

L: vertical distance of the two burner;

$|U_{fuel}|$: stream velocity of the fuel at the fuel boundary(cm/s);

$|U_{oxidizer}|$: stream velocity of the oxidizer at the oxidizer boundary (cm/s);

$\sqrt{\rho_{fuel}}$: density of fuel flow (g/cm^3);

$\sqrt{\rho_{oxidizer}}$: density of oxidizer flow (g/cm^3);

4.2.3 Gas sampling system

From previous study, some gas species including CH_4, N_2, O2, CO, C_2H_2, C_2H_4 and C_2H_6 were measured and analyzed by Gas Chromatography (GC)[98]. However, there is another important gas species nitric oxide (NO) which cannot be analyzed by using GC due to the detection limitation. Thus, Fourier transform infrared spectroscopy (FTIR) is introduced into the gas sampling system to analyze NO and CH_4 species.

4.2.3.1 Gas sampling procedures

In this study, the Thermo Scientific Nicolet 6700 FTIR connected with a TGA-Interface, as Figure 4-3showed, is used to measure NO and CH_4. It mainly consists of a laser, an infrared source, an interferometer, a detector, a series of mirrors and TGA-Interface with a gas cell inside. The gas cell had a path length of 100mm and a volume of 23mL. The sampling

system is shown in Figure 4-1. In order to minimize the effects of water on the NO peaks, a water removal device is employed before gas going into FTIR gas cell.

Figure 4-3Thermo Scientific Nicolet 6700 FTIR connected with a TGA-Interface

In the sampling process, a microprobe is inserted into the reaction zone; the gas sample is sucked into the gas line by a vacuum pump which is connected at the outlet of FTIR. In this process, the gas sample would flow through the gas cell at a vacuum pressure of -1psi. For each gas sample, to ensure enough gas samples in the gas cell, the sampling time for each position should be over 20mins. After obtaining stable gas sample, the spectrums are collected for each position.

4.2.3.2 Fourier transform infrared spectroscopy (FTIR)

Infrared spectrometers[99] have been widely used in a variety of applications including quantitative analysis of complex mixtures, biomedical and biological spectroscopy and investigation of interfacial phenomena, etc. To analyze the components and concentration of gas products from the combustion system, a gas sample should be subjected to infrared radiation at a multitude of frequencies to determine the frequencies at which the sample absorbs infrared radiation and the intensities of adsorption and the components and concentrations can be identified through analyzing the development of the adsorption frequency curve.

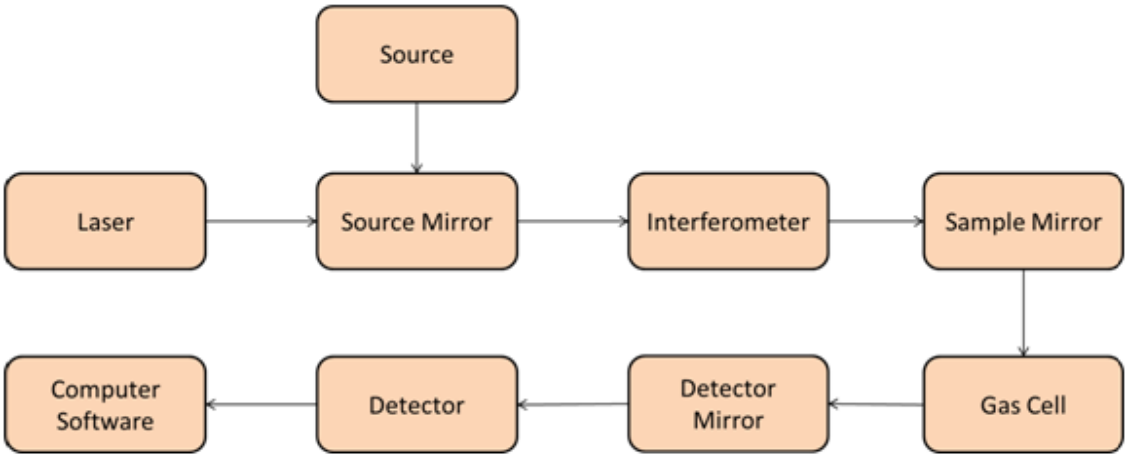

Figure 4-4 Schematic of FTIR

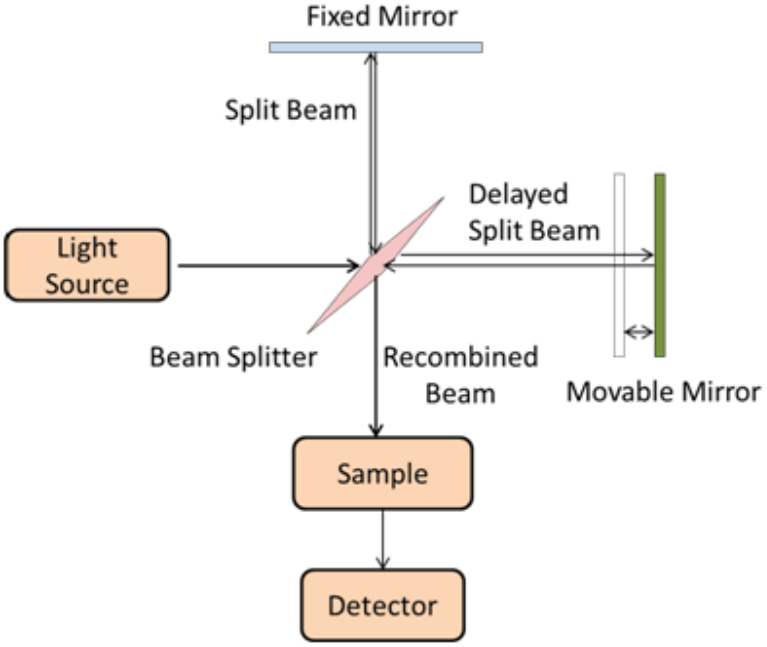

Figure 4-5 FTIR working theory

Figure 4-4 above showed the schematic of FTIR. FTIR consists of an infrared source, a laser, mirrors, an interferometer, sample cell, detector and the software. When gas passed

through the gas cell into the detector, the light would be absorbed or transmitted. Then, the signal is deconstructed by the software using the Fourier transform and an infrared spectrum is generated.

Figure 4-5 showed the operation of a Michelson interferometer. It consists of a fixed mirror, a movable mirror and a beam splitter which is based on potassium bromide (KBr) in our FTIR. The beam of radiation from the source is split to two: one is partially transmitted to the movable mirror and the other one partially reflected to the fixed mirror. The beams then return to the beam splitter where they interfere with each other. Thus, part of the beam intensity is directed to the sample cell and the rest returns to the source. The intensity of each beam depends on the difference in their path. The spectral information is obtained by the variation in the intensity of the beams reaching the detector as a function of path difference. The resulting signal is called an interferogram and contains all of the infrared frequencies present in the beam. After the beam exits the interferometer, it is deflected by a sample mirror prior to its entry into the sample cell.

The beam of infrared radiation is partially absorbed and transmitted when passing through the sample cell. The adsorption of radiation is a gain in energy association with quantum transition from one energy state to another. All the molecules can vibrate at their characteristic frequencies. When the molecules vibrate, they can absorb infrared radiation if the vibration produces a change in the dipole moment. However, some molecules cannot have an inherent dipole moment. For example, nitrogen molecule has no dipole moment as a result of the equal separation of charge in the molecule. The bond is stretched as vibrating, but the molecule has no dipole moment due to the separation of charge, which indicates that it cannot absorb infrared radiation. The noble gases (helium, argon) and diatomic molecules consisting of two identical atoms (oxygen, nitrogen and hydrogen) cannot absorb radiation, as explained. However, some molecules, like carbon dioxide, can absorb radiation without dipole moment in the beginning. This may be caused by the dipole change from the generation of the dipole moment during the vibration.

After the detector get the beam, the detector will use a sensor to process the infrared radiation and produce an electrical signal as a result. The interferogram is generated using the detector, as it records the infrared radiation that it receives over time. However, it can be affected by the instrument and atmospheric conditions. So it is necessary to collect one background interferogram without samples and one interferogram with samples. The difference of the two interferograms indicates the infrared radiation absorbed by the sample. And then the software can conduct a Fourier transformation on each interferogram, yielding energy curves which show the radiation reaching the detector as a function of frequency.

Equation 4-2 showed the relationship between transmission and the energy curves. And equation 4-3 showed the percent transmittance and absorbance relationship.

$$\boldsymbol{Transmission}(\%\,\boldsymbol{Transmittance}) = \frac{\boldsymbol{SampleEnergyCurve}}{\boldsymbol{BackgroundEnergyCurve}} \times \mathbf{100}\% \quad \textbf{(4-2)}$$

$$\boldsymbol{A} = -\boldsymbol{log}_{\mathbf{10}}[\frac{\%\,\boldsymbol{Transmittance}}{\mathbf{100}}] \quad \textbf{(4-3)}$$

Using FTIR, the components in the sample and concentrations can be determined by comparing the unknown spectrum with the known spectrum standards.To get the quantitative analysis of samples, there are variety methods for FTIR, such as Beer's law, classical least squares and partial least squares, etc[100]. In this study, the CLS analysis method was employed. The gas model includes NO and CH_4.

The classical least squares (CLS) method assumed that the absorption is a sum of the absorption contributions of each of the components in the sample at a particular wave number. The relationship between absorbance and concentration is showed in the equation.

$$\boldsymbol{A}(\boldsymbol{w_i}) = \boldsymbol{a_x}(\boldsymbol{w_i})\boldsymbol{bc_x} + \boldsymbol{a_y}(\boldsymbol{w_i})\boldsymbol{bc_y} + \boldsymbol{a_z}(\boldsymbol{w_i})\boldsymbol{bc_z} + \cdots + \boldsymbol{E}(\boldsymbol{w_i}) \quad \textbf{(4-4)}$$

$A(w_i)$:total absorbance at wave number w_i ,

E: the residual error from linear-squares regression;

x, y and z: components in the sample.

By using CLS analysis, a larger number of standard spectrums are required. It can handle component absorptions that extend beyond a single peak and overlap considerably. However, CLS cannot handle impurities. In the CLS method, the absorption at a particular wave number is a sum of the absorption contributions of each of the components, so the equation is invalid when one or more components are not incorporated in the calibration model. Thus, all components in the sample must be included in the calibration model, which can make calibration difficult due to the large number of gas components in the sample.

In the calibration process, gas mixtures with different concentrations of CH_4 and NO were sent into the FTIR system directly from gas cylinders by using mass flow controller to control the flow rate for each gas. For all the calibration process, the gas cell temperature was set to be 200°C and the gas cell was purified with nitrogen. During the spectrum collecting process, the gas flow into the gas cell continuously at a certain flow rate with known concentration. OMNIC [101]was used to collect the sample spectrums for each standard. A total number of 30spectrums were collected for the calibration (CH_4 range: 1%-15%; NO range: 10ppm-300ppm). TQ analyst was used to analyze all the calibration standards and develop the calibration model. After the calibration curves obtained, the quantitative analysis of each gas sample can be conducted by import gas sample spectrums to the TQ analyst model and get gas components information.

4.3 Numerical setup

CHEMKIN-Pro is employed to study the non-catalytic and catalytic natural gas combustion process on the counter flow burner numerically.

4.3.1 Numerical model description

The geometry of the counter flow burner in the numerical setup is showed in Figure 4-6.It consists of two separated burners with the gap of 2 cm. The diameter of the burners is 6cm, which is to say r = 3cm. As indicated in the figure, the oxidizer, including air and oxygen, flows into the burner from the top side with a total velocity u_o=7.94 cm/s; the fuel, including methane and nitrogen; flows into the burner from the bottom side with a total velocity of

u_f=8.35 cm/s. The detailed composition is shown in the Table. The calculated overall equivalence ratio is 0.5.

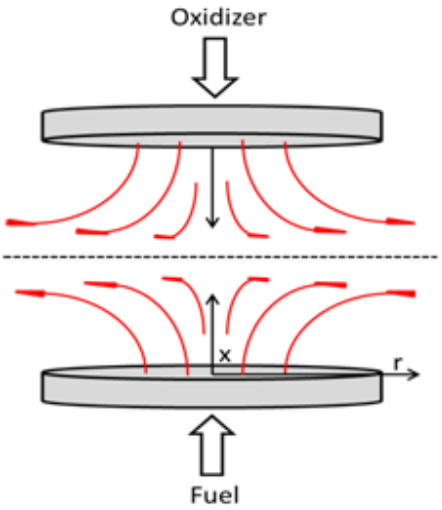

Figure 4-6 Configuration of flame model in numerical calculation

Table 4-2 Composition of fuel/air flows

Oxidizer			Fuel		
O2%	N2%	flow rate (cm/s)	CH4%	N2%	flow rate (cm/s)
0.409	0.591	7.94	0.097	0.903	8.35

4.3.2 Governing equation

The opposed flow flame model[94] of CHEMKIN is used to simulate the counter flow flame. The opposed flow flame simulator is derived from the model originally developed by Kee, et al.[102]. The axisymmetric coordinates was employed. The species diffusion velocities were computed using the mixture-average diffusivity including the thermal

diffusion coefficient. The plateau profiles for initial conditions were employed and maximum temperature for the initial profile was set to be 2200K.

At steady state, conservation of mass is defined as:

$$\frac{\partial(\rho u)}{\partial x}+\frac{1}{\xi^{-2}}\frac{\partial(\rho v_{\xi}\xi^{n-2}}{\partial \xi}=0 \quad \textbf{(4-5)}$$

u: axial velocity components;

v_{ξ}: radial velocity components;

ρ:the mass density.

It is found that v_{ξ}/ξ and other variables are the functions of x only. Two functions are defined as:

$$G(x)=\frac{-(\rho v_{\xi})}{\xi} \quad \textbf{(4-6)}$$

$$F(x)=\frac{\rho u}{(n-1)} \quad \textbf{(4-7)}$$

And then the equation can be reduced to

$$G(x)=\frac{dF(x)}{dx} \quad \textbf{(4-8)}$$

For the axial velocity u, since F and G are functions of x only, so are ρ, u, T and Y_k.

The perpendicular momentum equation is satisfied by the eigenvalue

$$H=\frac{1}{\xi^{n-2}}\frac{\partial p}{\partial \xi}=constant \quad \textbf{(4-9)}$$

The perpendicular momentum equation is

$$H-(n-1)\frac{d}{dx}\left(\frac{FG}{\rho}\right)+\frac{nG^2}{\rho}+\frac{d}{dx}\left[\mu\frac{d}{dx}\left(\frac{G}{\rho}\right)\right]=0 \quad \textbf{(4-10)}$$

Energy and species conservation are

$$\rho u\frac{dT}{dx}-\frac{1}{c_P}\frac{d}{dx}\left(\lambda\frac{dT}{dx}\right)+\frac{\rho}{c_P}\sum_k c_{Pk}Y_k V_K\frac{dT}{dx}+\frac{1}{c_P}\sum_k h_k\dot{\omega}_k+\frac{1}{c_P}\dot{Q}_{rad}=0 \quad \textbf{(4-11)}$$

where$\dot{Q}_{rad}$ is the heat loss due to gas and particle radiation.

$$\boldsymbol{\rho u \frac{dY_k}{dx} + \frac{d}{dx}(\rho Y_k V_k) - \dot{\omega}_k W_k = 0 \;\; k = 1, \ldots, K} \quad \textbf{(4-12)}$$

where the diffusion velocities are given by the mixture-averaged formulation.

$$\boldsymbol{V_k = -\frac{1}{X_k} D_{km} \frac{dX_k}{dx} - \frac{D_k^T}{\rho Y_k} \frac{1}{T} \frac{dT}{dx}} \quad \textbf{(4-13)}$$

$$\boldsymbol{D_{km} = \frac{1 - Y_k}{\sum_{j \neq k}^{K} \frac{X_j}{\mathfrak{D}_{jk}}}} \quad \textbf{(4-14)}$$

D_{km} , $\mathfrak{D}_{jk}$ and D_k^T are the mixture-average, binary and thermal diffusion coefficients, respectively.

The boundary conditions for the fuel and oxidizer streams at the nozzles are

$$\boldsymbol{x = 0: F = \frac{\rho_F u_F}{(n-1)}; G = 0; T = T_F; \; \rho u Y_k + \rho Y_k V_k = (\rho u Y_k)_F} \quad \textbf{(4-15)}$$

$$\boldsymbol{x = L: F = \frac{\rho_O u_O}{(n-1)}; G = 0; T = T_O; \; \rho u Y_k + \rho Y_k V_k = (\rho u Y_k)_O} \quad \textbf{(4-16)}$$

4.3.3 Chemical Kinetics

In the simulation, GRI-Mech 3.0 schemes are employed for the gas phase mechanism. GRI-Mech3.0 schemes include 53 species and 325 reactions. The species transport properties are calculated from CHEMKIN database. Gas phase reaction rates were evaluated using CHEMKIN.

4.4 Results and Discussion

In this section, the modeling results are compared with experimental results in methane combustion process on the counter flow. Various gas species are studied, including CH_4, O_2, N_2, CO, C_2H_2, C_2H_4, C_2H_6 and NO.

4.4.1 Species analysis along vertical direction

Figure 4-7 showed methane profile along with the vertical distance of the two separated burners. When approaching flame, methane starts to react and the amount of methane decreases. After reaching the flame plane, methane concentration is reduced sharply and almost completely reacted after going through the flame. The modeling results predict almost the same profile of methane and showed good agreement with data from experiments.

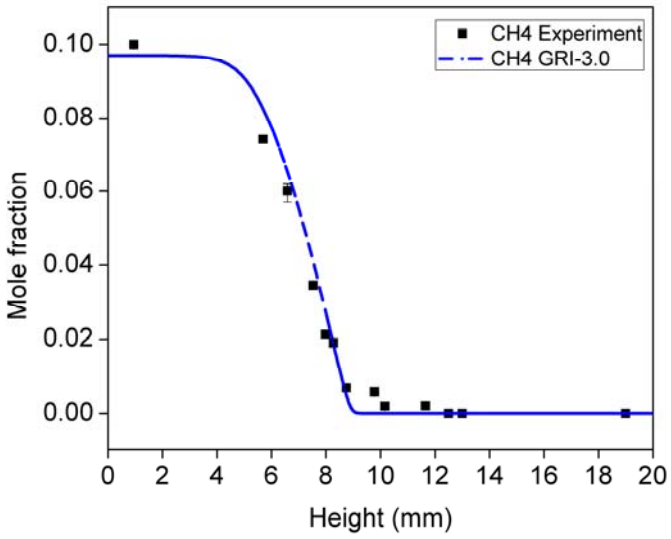

Figure 4-7 Experimental and numerical profile of CH_4 (zero point at x axis indicates the beginning of the bottom burner)

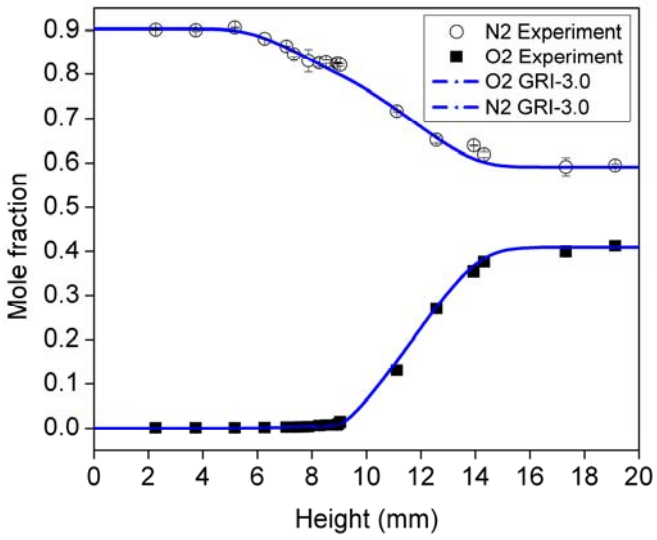

Figure 4-8 Experimental and numerical profile of N_2 and O_2

As O_2 and N_2 are the main components in the air, they are abundant in the whole reaction zone. The profiles of them were plotted below to study the oxidizer conditions. The experimental data are from the previous study [103]. The GRI-Mech 3.0 mechanism predicts similar results of N_2 and O_2 compared to experimental data. Throughout the reaction zone, the modeling data still showed great agreement with experimental results.

As CO is one of the main pollutant gas and incomplete combustion products. The production condition of CO is measured in the experiments and also in the numerical study. The profile of CO is plotted in Figure 4-10. As indicated in the figure, the concentration of CO reached to its maximum value (near 0.016) at the flame zone from experiments[103]. The predicted profiles from numerical study also had the peak values at the same location (h=8.8mm). However, the GRI-Mech 3.0 mechanism under-predicted the CO level compared with the experimental data. In the modeling process, the ideal reactions are assumed. While, in the real experiments, the reactants may not reacts completely as the transport and heat transfer conditions are not perfect.

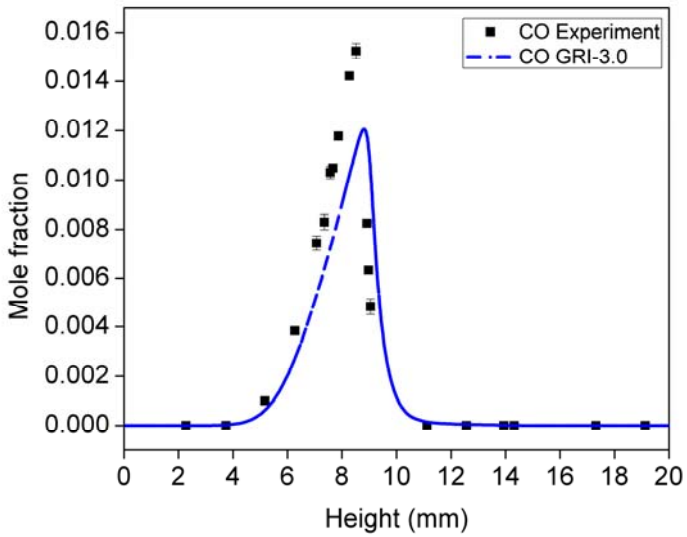

Figure 4-9 Experimental and numerical profile of CO

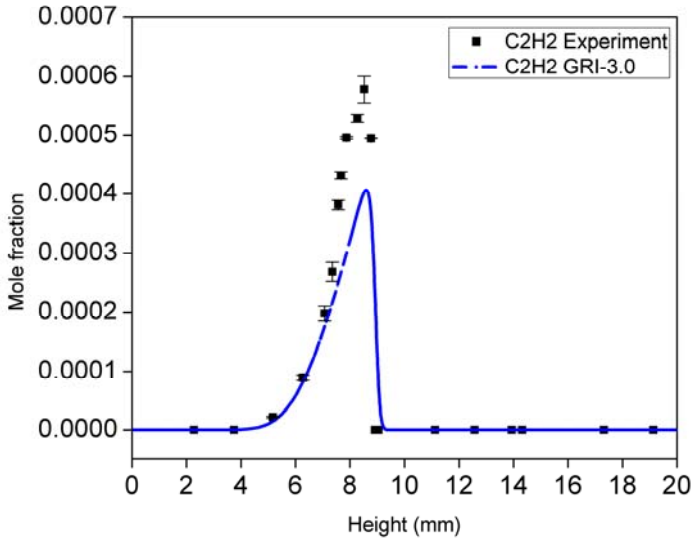

Figure 4-10 Experimental and numerical profile of C_2H_2

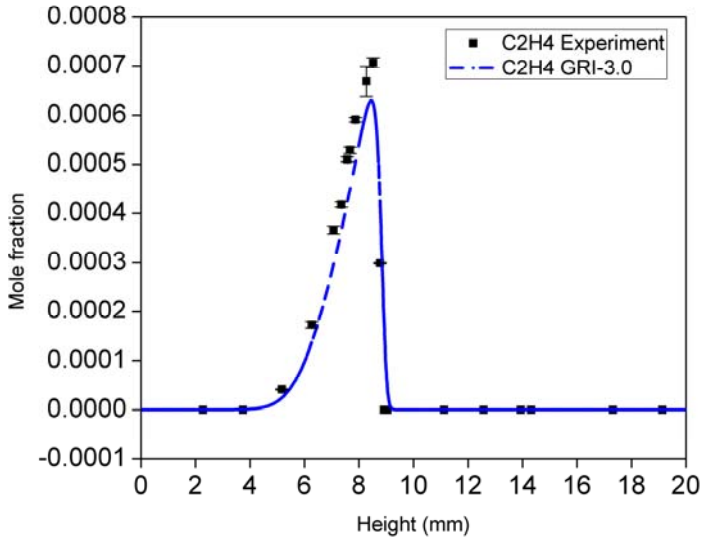

Figure 4-11 Experimental and numerical profile of C_2H_4

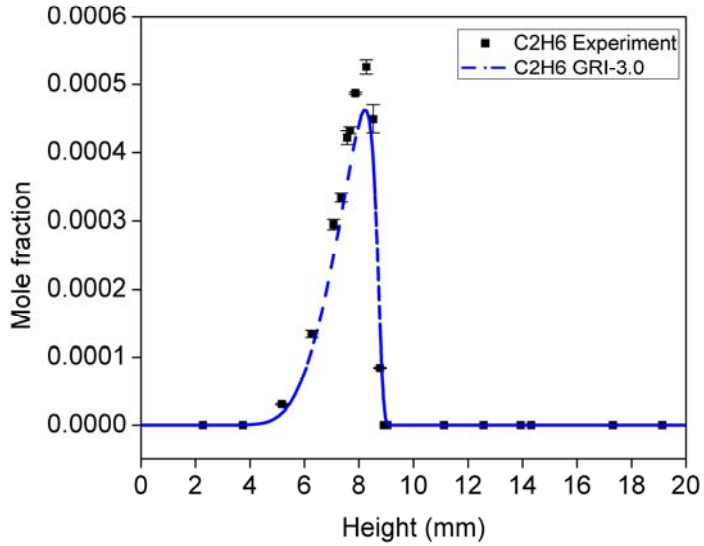

Figure 4-12 Experimental and numerical profile of C_2H_6

The hydrocarbons are another main pollutant produced in the combustion process. In this study, three C2 hydrocarbons (C_2H_2, C_2H_4 and C_2H_6) are analyzed. Figures from 4-10 to 4-12 illustrate the hydrocarbon emissions. All the three hydrocarbons started to be generated from the fuel side and gradually increased. The peak values located at the flame zone and sharply decreased to almost zero after the flame zone at the oxidizer side. The peak values for C_2H_2, C_2H_4 and C_2H_6 are around 600ppm, 740ppm and 550ppm, respectively [103]. In the modeling process, GRI-Mech 3.0 gives similar generation trends but under-predicts all the three hydrocarbons emissions.

NO profile is plotted in Figure 4-13. As shown, similar with other emission species profiles, NO production starts in the middle part of the reaction zone and reach to its maximum value (32ppm) at h= 9.7mm. The distance where NO maximum value presented is slightly higher than other emissions peak positions. NO formation in methane combustion system is mainly through thermal pathway. Thus, the maximum value of NO should be at the maximum temperature position, which is in the flame zone. While, other emissions, such as CO, C_2H_2, C_2H_4 and C_2H_6, usually present more in the fuel rich zone (fuel side).

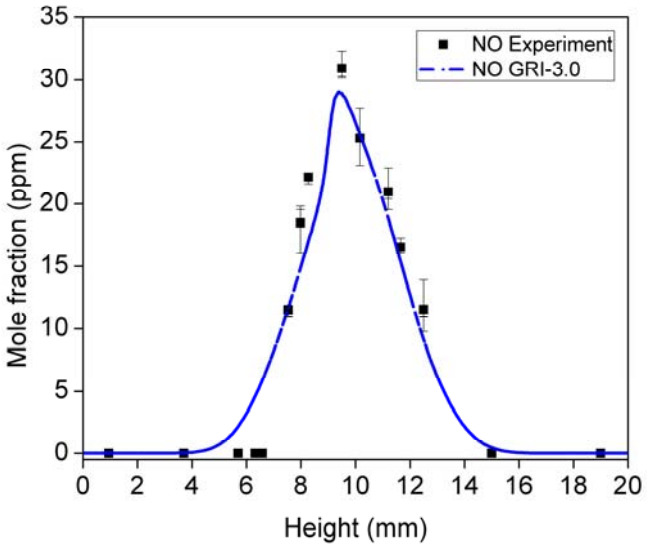

Figure 4-13 Experimental and numerical profile of NO

4.4.2 Species analysis along horizontal direction

The flame condition is assumed to be constant along the same horizontal level ideally. However, in real experiments, many factors, such as heat transfer and effects from surroundings, can affect the present flame conditions. Thus, reviewing the gas profiles along the horizontal direction is important. Figure 4-14 and Figure 4-15 are showing the gas profiles of CH_4 and NO from the first flow condition, respectively. The gas samples are collected at the height of 8mm, where the NO level is relatively high.

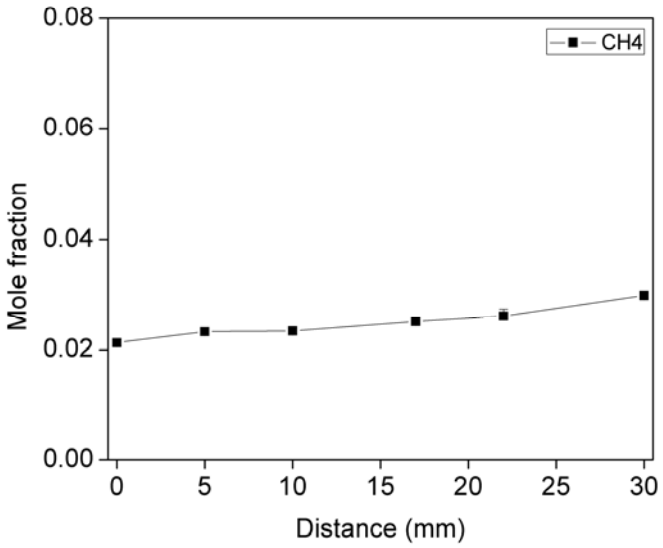

Figure 4-14 CH4 profile in the horizontal direction (zero point in x-axis indicates the central vertical axis)

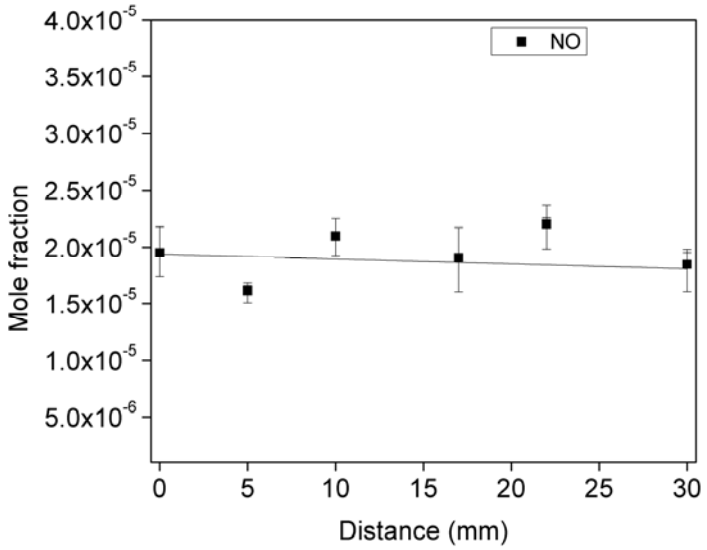

Figure 4-15 NO profile in the horizontal direction (zero point in x-axis indicates the central vertical axis)

As Figure 4-14 shown, CH_4 concentration increased slightly as the sample position moved to the edge of the burner. This result corresponds to the heat transfer conditions. As temperature at the edge is lower than that at the center, less CH_4 is reacted. While, the NO profile shows different trend, which have a slightly decreased when moving to the edge. NO is one of the product when high combustion temperature generated. When moving to the edge, NO level decreased due to the decreasing temperature. However, overall, the species level of CH_4 and NO are not affected by the horizontal sampling position a lot.

4.4.3 Effect of fuel/oxidizer ratio on NO production

To study the effects of different fuel levels on the NO production, three flow conditions are evaluated. The CH_4 flow rates are 1.4 L/min, 1.8 L/min and 2.2 L/min. In the experiments, the oxidizer (oxygen and air) flow conditions are kept constant. N_2 flow is adjusted to balance the flow rate and a constant strain rate is kept for the three conditions.

During the experiments, the color of the flame becomes darker when increasing CH_4 flow rate. In other words, more stable flame is obtained as CH_4 increasing.

The measured NO profile is shown in Figure 4-16. The maximum NO production increased from 32ppm to 180ppm (around 5 times) when CH_4 flow rate increases from 1.4 to 2.2 (less than 2 times). NO is mainly produced from thermal mechanism in this system. More NO is generated when temperature is higher. When increasing fuel concentration, more heat is generated and flame temperature goes up significantly. In any cases, the maximum NO concentration is located at the flame sheet where the temperature is the highest.

Based on this analysis, to control the NO emission, the fuel/oxidizer ratio is important. Theoretically, the less concentration of CH_4, the less NO is formed. However, considering the stability of the flame, there should be a limit for reducing the fuel concentration.

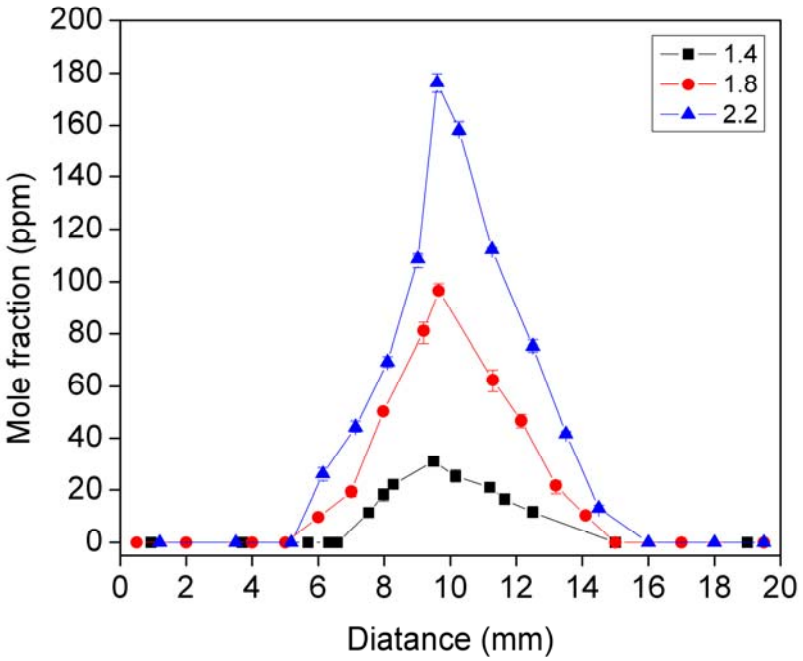

Figure 4-16 NO profiles from different fuel and oxidizer ratios (zero point in x-axis is at the surface of bottom burner)

4.4.4 Uncertainty analysis

The error present in the experiments and the discrepancies between the experiment and model prediction may be caused by several sources of error.

4.4.4.1 Experimental analysis

The errors present in the experimental results may be caused by both the system uncertainties and the experimental operations.

In the experimental system, the mass flow controller, FTIR and pressure gauge can cause some errors. The error caused by FTIR is considered to be less than 5%, according to the calibration results. For the mass flow controllers, the errors are 1% of the experimental readings and 2% of the full scales, respectively. For the pressure gauge, the errors are 1% of the experimental readings and 0.5% of the full scales.

The experimental setup, operation and gas sampling method can also lead to the experimental uncertainties. The two burners of the counter-flow burner system are separated at a distance of 20mm, ideally, whereas the actually distance is a little smaller caused by the manufacture tolerance. During the sampling process, the reactants may still remain reacting for a short time which can cause some error. When measuring the sampling position, a caliper is employed to get the position information manually, which can introduce part of the errors. In addition, when quantifying the experimental spectrum using FTIR, ideal gas law is used to adjust the pressure difference between the calibration and experiments. The error can be present during the converting process. Last, the reaction system of counter-flow burner is an open system exposed to the surrounding experiment. The surrounding air flux caused by operator and fumehood will affect the structure of flame, which will cause uncertainties in the experimental measurements.

4.4.4.2 Modeling uncertainties

Errors in the present model may result from the reaction mechanism, uncertainties from reaction rate constants, thermochemical data, transport properties and geometry difference between numerical model and actual instrument.

GRI-Mech 3.0 schemes includes 53 species and 325 elementary reactions. It is designed to model natural gas combustion. During the modeling process, all the reaction parameters and heat and mass transfer conditions are assumed to be ideally present. However, in the actual experimental process, there are a lot of factors that can affect the reaction results, such as surroundings temperature and air flux, etc.

As mentioned in the burner geometry description, there is a central port (diameter: 1/8 inch) at the bottom burner. In this study, there is no catalyst and additives insert, which means no gas flow from the central port. However, in the numerical model, there is no central port defined. The geometry difference can cause the disagreement between numerical model and experiments.

4.5 Summary

The characteristics of natural gas combustion on the counter-flow flame burner are numerically and experimentally investigated. The gas species profiles from experiments are compared with model results. The effects of three different fuel concentrations on NO production are evaluated.

Overall, the numerical predictions are consistent with experimental results, that means the model can be used to predict the gas species of natural gas combustion: the model can predict the major gas species accurately; however, the numerical model under-predicts the emission levels. The comparison of NO production from different fuel levels indicates that higher fuel level will generate more NO product due to higher flame temperature under fuel lean conditions.

Chapter 5
Conclusions and Recommendations

5.1 Conclusions

I) The hydrogen enriched natural gas combustion in the channel reactor is numerically studied via CHEMKIN. The effects of hydrogen addition, Pt-catalyst, temperature and different gas and surface mechanisms on the ignition and NO formation are evaluated.

The planar channel shear-layer flow reactor model of CHEMKIN is used with GRI-Mech 3.0 scheme as gas phase mechanism and Deutschmann scheme as surface mechanism. Four different flow conditions including various H_2 concentrations are used in both the catalytic and non-catalytic combustion process. During the numerical study, the temperature and OH species are used to evaluate the ignition condition. NO profiles are plotted for different conditions. In addition, effects of wall temperature and inlet flow temperature are studied. Several different gas mechanisms and surface mechanisms are employed in order to study the ignition and species difference.

The modeling results show that hydrogen can promote CH_4 ignition significantly and reduce NO formation in the non-catalytic combustion. With Pt-catalyst present, the effects of hydrogen are not obvious due to lower reaction temperature. Pt-catalyst can reduce both the reaction temperature and NO production a lot. Through the temperature study, both higher wall temperature and inlet flow temperature can promote ignition occurring. Several different gas and surface mechanism are employed. By employing different mechanism, the obtained ignition and species conditions are very different. However, to determine which mechanism suitable for the actual condition is still remained to be confirmedwith experiments.

II) The characteristics of natural gas combustion on the counter-flow flame burner are numerically and experimentally investigated. The gas species profiles from experiments are compared with model results. The effects of three different fuel concentrations on NO production are evaluated.

In the experimental system, the combustion occurred on the counter-flow flame burner and FTIR is used to measure CH_4 and NO concentration. In the numerical study, an opposed flame model from CHEMKIN is employed. Some experimental data of other gas species (N_2, O_2, CO, C_2H_2, C_2H_4 and C_2H_6) from previous work are used to evaluate the numerical model.

Overall, the numerical results are consistent with experimental results, that means the model can be used to predict the gas species of the natural gas combustion. The model can predict the major gas species accurately. However, the numerical model under-predicts the emission levels. A comparison of NO production from different fuel levels is conducted, which implies that higher fuel level will generate more NO product due to higher flame temperature under fuel lean conditions.

5.2 Recommendations

Some recommendations are suggested to improve the quality of results discussed in this study and future work.

I) In the counter-flow flame experiments, the calibration of FTIR is limited to 2 species in this study. If more gas components can be added into the calibration model, more accurate results can be obtained.

II) The numerical model of the counter-flow burner in CHEMKIN doesn't include the central port on the bottom burner present in actual experiments. Maybe some other software, such as FLUENT, can be employed to include more detailed model.

III) The flame temperature is not obtained in this study. Temperature is a very import factor for NO study, since NO formation is directly related to flame temperature. In the future experiments, a temperature measuring device can be considered for the experimental system.

IV) The natural gas combustion in the channel reactor is only studied numerically. In some degree, it is hard to evaluate the model performance and the different mechanisms

without experimental data.The experimental work is expected to be conducted in order to validate the modeling work.

References

[1] S. O. Akansu, N. Kahraman and B. Çeper, "Experimental study on a spark ignition engine fuelled by methane–hydrogen mixtures," *Int J Hydrogen Energy,* vol. 32, pp. 4279-4284, 12, 2007.

[2] J. Park, H. Cha, S. Song and K. M. Chun, "A numerical study of a methane-fueled gas engine generator with addition of hydrogen using cycle simulation and DOE method," *Int J Hydrogen Energy,* vol. 36, pp. 5153-5162, 4, 2011.

[3] M. M. Abdelaal and A. Hegab, "Combustion and emission characteristics of a natural gas-fueled diesel engine with EGR," *Energy Convers. Manage.,* vol. 64, pp. 301-312, Dec 1, 2012, 2012.

[4] F. Moreno, J. Arroyo, M. Muñoz and C. Monné, "Combustion analysis of a spark ignition engine fueled with gaseous blends containing hydrogen," *Int J Hydrogen Energy,* vol. 37, pp. 13564-13573, 9, 2012.

[5] C. G. Bauer and T. W. Forest, "Effect of hydrogen addition on the performance of methane-fueled vehicles. Part I: effect on S.I. engine performance," *Int J Hydrogen Energy,* vol. 26, pp. 55-70, 1, 2001.

[6] B. J. Lowesmith and G. Hankinson, "Large scale experiments to study fires following the rupture of high pressure pipelines conveying natural gas and natural gas/hydrogen mixtures," *Process Saf. Environ. Prot.,* vol. 91, pp. 101-111, Mar 1, 2013, 2013.

[7] I. A. Gondal and M. H. Sahir, "Prospects of natural gas pipeline infrastructure in hydrogen transportation," *Int. J. Energy Res.,* vol. 36, pp. 1338-1345, 2012.

[8] O. Deutschmann, L. I. Maier, U. Riedel, A. H. Stroemman and R. W. Dibble, "Hydrogen assisted catalytic combustion of methane on platinum," *Catalysis Today,* vol. 59, pp. 141-150, 6/10, 2000.

[9] D. Ciuparu, M. R. Lyubovsky, E. Altman, L. D. Pfefferle and A. Datye, "Catalytic combustion of methane over palladium-based catalysts," *Catalysis Reviews,* vol. 44, pp. 593-649, 2002, 2002.

[10] P. Forzatti, "Status and perspectives of catalytic combustion for gas turbines," *Catalysis Today,* vol. 83, pp. 3-18, 8/15, 2003.

[11] W. May and E. Hirs, "Catalyst for improving the combustion efficiency of petroleum fuels in diesel engines," in *11th Diesel Engine Emissions Reduction Conference,* 2005, pp. 1-16.

[12] EIA,"Natural gas prospects to 2010," 1998.

[13] EIA, "Natural Gas Issues and Trends," 1998.

[14] G. Karavalakis, T. D. Durbin, M. Villela and J. W. Miller, "Air pollutant emissions of light-duty vehicles operating on various natural gas compositions," *Journal of Natural Gas Science and Engineering,* vol. 4, pp. 8-16, 1, 2012.

[15] M. Hajbabaei, G. Karavalakis, K. C. Johnson, L. Lee and T. D. Durbin, "Impact of natural gas fuel composition on criteria, toxic, and particle emissions from transit buses equipped with lean burn and stoichiometric engines," *Energy,* vol. 62, pp. 425-434, 12/1, 2013.

[16] A. Lewandowska, I. Kocemba and J. Rynkowski, "Catalytic Properties of Ag/SnO2 Catalysts Applied in Low-Temperature Methane Oxidation," *Polish J. of Environ. Stud.,* vol. 17, pp. 433-437, 2008.

[17] J. López-Herce, R. Borrego, A. Bustinza and A. Carrillo, "Elevated carboxyhemoglobin associated with sodium nitroprusside treatment," *Intensive Care Med.,* vol. 31, pp. 1235-1238, 2005.

[18] M. M. Abdelaal and A. H. Hegab, "Combustion and emission characteristics of a natural gas-fueled diesel engine with EGR," *Energy Conversion and Management,* vol. 64, pp. 301-312, 12, 2012.

[19] Y. Wang, Y. Liu, Q. Cao, C. Wang and D. Che, "Homogeneous Combustion of Fuel Ultra-Lean Methane–Air Mixtures: Experimental Study and Simplified Reaction Mechanism," *Energy & Fuels,* vol. 25, pp. 3437-3445, 2011.

[20] A. Indarto, "Soot Growth Mechanisms from Polyynes," *ENVIRONMENTAL ENGINEERING SCIENCE,* vol. 26, pp. 1685-1691, 2009.

[21] A. V. Krestinin, "Detailed modeling of soot formation in hydrocarbon pyrolysis," *Combust. Flame,* vol. 121, pp. 513-524, 3, 2000.

[22] I. Glassman and R. A. Yetter, *Combustion- Fourth Edition.* US: Academic Press, 2008.

[23] N. M. Marinov, W. J. Pitz, C. K. Westbrook, A. E. Lutz, A. M. Vincitore and S. M. Senkan, "Chemical kinetic modeling of a methane opposed-flow diffusion flame and comparison to experiments," *Symp Int Combust,* vol. 27, pp. 605-613, 1998.

[24] Y. R. Sivathanu and J. P. Gore, "Effects of gas-band radiation on soot kinetics in laminar methane / air diffusion flames," *Combust. Flame,* vol. 110, pp. 256-263, 7, 1997.

[25] R. E. Hayes and S. Kolaczkowski, *Introduction to Catalytic Combustion.* UK: Gordon and Breach Science Publishers, 1997.

[26] P. C. Malte and D. T. Pratt, "The role of energy-releasing kinetics in NOx formation: fuel-lean, jet-stirred CO-air combustion," *Combustion Sci. Technol.,* vol. 9, pp. 221-231, 01/01; 2013/07, 1974.

[27] G. Löffler, R. Sieber, M. Harasek, H. Hofbauer, R. Hauss and J. Landauf, "NOx formation in natural gas combustion—a new simplified reaction scheme for CFD calculations," *Fuel,* vol. 85, pp. 513-523, 3, 2006.

[28] R. S. Barlow, A. N. Karpetis, J. H. Frank and J. -. Chen, "Scalar profiles and NO formation in laminar opposed-flow partially premixed methane/air flames," *Combust. Flame,* vol. 127, pp. 2102-2118, 11, 2001.

[29] C. T. Bowman, R. K. Hanson, D. F. Davidson, W. C. Gardiner Jr., V. Lissianski, G. P. Smith, D. M. Golden, M. Frenklach and M. Goldenberg, "http://diesel.me.berkeley.edu/~gri_mech/new21/version21/text21.html," 1995.

[30] G. P. Smith, D. M. Golden, M. N. Frenklach, W. Moriarty, B. Eiteneer, M. Goldenberg, C. T. Bowman, R. K. Hanson, S. Song, W. C. Gardiner Jr., V. V. Lissianski and Z. Qin, "http://www.me.berkeley.edu/gri_mech/," 1999.

[31] J. A. Miller and C. T. Bowman, "Mechanism and modeling of nitrogen chemistry in combustion," *Progress in Energy and Combustion Science,* vol. 15, pp. 287-338, 1989.

[32] U. Kesgin, "Study on prediction of the effects of design and operating parameters on NOx emissions from a leanburn natural gas engine," *Energy Conversion and Management,* vol. 44, pp. 907-921, 4, 2003.

[33] R. Kapaku, "Effects of Inlet Pressure and Temperature, and Fuel-Air Equivalence Ratio on Natural Gas Combustion Utilizing the GRI Mech 3.0 Chemical Kinetics Mechanism," *The Ohio State University,* 2012.

[34] E. Navarro, T. J. Leo and R. Corral, "CO2 emissions from a spark ignition engine operating on natural gasand hydrogen blends (HCNG)," *Appl. Energy,* vol. 101, pp. 112-120, Jan 1, 2013, 2013.

[35] M. Bysveen, "Engine characteristics of emissions and performance using mixtures of natural gas and hydrogen," *Energy (Oxf.),* vol. 32, pp. 482-489, Apr 2007, 2007.

[36] K. Zhao, D. Cui, T. Xu, Q. Zhou, S. Hui and H. Hu, "Effects of hydrogen addition on methane combustion," *Fuel Process Technol,* vol. 89, pp. 1142-1147, 2008.

[37] J. Phillips and R. Roby, "Hydrogen-enriched natural gas offers economic NOx reduction alternative," *Power Eng (Barrington, Illinois),* vol. 104, pp. 3, 2000.

[38] S. Allenby, W. -. Chang, A. Megaritis and M. L. Wyszynski, "Hydrogen enrichment: A way to maintain combustion stability in a natural gas fuelled engine with exhaust gas recirculation, the potential of fuel reforming," *Proc. Inst. Mech. Eng. Pt. D: J. Automobile Eng.,* vol. 215, pp. 405-418, 2001.

[39] F. Halter, C. Chauveau and I. Gökalp, "Characterization of the effects of hydrogen addition in premixed methane/air flames," *Int J Hydrogen Energy,* vol. 32, pp. 2585-2592, 9, 2007.

[40] F. Ma, H. Liu, Y. Wang, Y. Li, J. Wang and S. Zhao, "Combustion and emission characteristics of a port-injection HCNG engine under various ignition timings," *Int J Hydrogen Energy,* vol. 33, pp. 816-822, 1, 2008.

[41] Y. Zhang, Z. Huang, L. Wei and S. Niu, "Experimental and kinetic study on ignition delay times of methane/ hydrogen/ oxygen/ nitrogen mixtures by shock tube," *Chinese Science Bulletin,* vol. 56, pp. 2853-2861, 2011.

[42] S. Cimino, A. Di Benedetto, R. Pirone and G. Russo, "CO, H2 or C3H8 assisted catalytic combustion of methane over supported LaMnO3 monoliths," *Catalysis Today,* vol. 83, pp. 33-43, 8/15, 2003.

[43] T. Korakianitis, A. M. Namasivayam and R. J. Crookes, "Natural-gas fueled spark-ignition (SI) and compression-ignition (CI) engine performance and emissions," *Progress in Energy and Combustion Science,* vol. 37, pp. 89-112, 2, 2011.

[44] C. N. Satterfield, *Heterogeneous Catalysis in Industrial Practice, 2nd Edition.* New York: Mcgraw-Hill Inc, 1991.

[45] J. Warnatz, U. Maas and R. W. Dibble, *Combustion: Physical and Chemical Fundamentals, Modeling and Simulation, Experiments, Pollutant Formation, 4th Edition.* New York: Springer Berlin Heidelberg, 2006.

[46] S. T. Aruna and A. S. Mukasyan, "Combustion synthesis and nanomaterials," *Current Opinion in Solid State and Materials Science,* vol. 12, pp. 44-50, 0, 2008.

[47] S. S. Gill, A. Tsolakis, K. D. Dearn and J. Rodríguez-Fernández, "Combustion characteristics and emissions of Fischer–Tropsch diesel fuels in IC engines," *Progress in Energy and Combustion Science,* vol. 37, pp. 503-523, 8, 2011.

[48] A. Srinivasan and C. Depcik, "Review of chemical reactions in the NO reduction by CO on rhodium/alumina catalysts," *Catalysis Reviews: Science and Engineering,* vol. 52, pp. 462-493, October-December 2010, 2010.

[49] S. Feng, W. Yang and Z. Wang, "Synthesis of porous NiFe2O4 microparticles and its catalytic properties for methane combustion," *Materials Science and Engineering: B,* vol. 176, pp. 1509-1512, 11/15, 2011.

[50] X. Guo, P. Brault, G. Zhi, A. Caillard, G. Jin and X. Guo, "Structural evolution of plasma-sputtered core–shell nanoparticles for catalytic combustion of methane," *J. Phys. Chem. C,* vol. 115, pp. 24164-24171, 2011.

[51] S. A. Shahamiri and I. Wierzba, "Simulation of catalytic oxidation of lean hydrogen–methane mixtures," *Int J Hydrogen Energy,* vol. 34, pp. 5785-5794, 7, 2009.

[52] C. Appel, J. Mantzaras, R. Schaeren, R. Bombach, A. Inauen, B. Kaeppeli, B. Hemmerling and A. Stampanoni, "An experimental and numerical investigation of homogeneous ignition in catalytically stabilized combustion of hydrogen/air mixtures over platinum," *Combust. Flame,* vol. 128, pp. 340-368, 3, 2002.

[53] R. Schwiedernoch, S. Tischer, O. Deutschmann and J. Warnatz, "Experimental and numerical investigation of the ignition of methane combustion in a platinum-coated honeycomb monolith," *Proceedings of the Combustion Institute,* vol. 29, pp. 1005-1011, 2002.

[54] M. Reinke, J. Mantzaras, R. Bombach, S. Schenker and A. Inauen, "Gas phase chemistry in catalytic combustion of methane/air mixtures over platinum at pressures of 1 to 16 bar," *Combust. Flame,* vol. 141, pp. 448-468, 6, 2005.

[55] J. H. Lee and D. L. Trimm, "Catalytic combustion of methane," *Fuel Process Technol,* vol. 42, pp. 339-359, 4, 1995.

[56] D. Trimm, "Catalytic combustion (review)," *Applied Catalysis,* vol. 7, pp. 249-282, 9/15, 1983.

[57] N. Imanaka, T. Masui and K. Yasuda, "Environmental catalysts for complete oxidation of volatile organic compounds and methane," *Chemistry Letters,* vol. 40, pp. 780-785, 2011.

[58] T. V. Choudhary, S. Banerjee and V. R. Choudhary, "Catalysts for combustion of methane and lower alkanes," *Applied Catalysis A: General,* vol. 234, pp. 1-23, 8/8, 2002.

[59] O. Demoulin, B. Le Clef, M. Navez and P. Ruiz, "Combustion of methane, ethane and propane and of mixtures of methane with ethane or propane on Pd/γ-Al2O3 catalysts," *Applied Catalysis A: General,* vol. 344, pp. 1-9, 7/15, 2008.

[60] M. Salaün, A. Kouakou, S. Da Costa and P. Da Costa, "Synthetic gas bench study of a natural gas vehicle commercial catalyst in monolithic form: On the effect of gas composition," *Applied Catalysis B: Environmental,* vol. 88, pp. 386-397, 5/20, 2009.

[61] P. Gélin, L. Urfels, M. Primet and E. Tena, "Complete oxidation of methane at low temperature over Pt and Pd catalysts for the abatement of lean-burn natural gas fuelled vehicles emissions: influence of water and sulphur containing compounds," *Catalysis Today,* vol. 83, pp. 45-57, 8/15, 2003.

[62] V. Meeyoo, D. L. Trimm and N. W. Cant, "The effect of sulphur containing pollutants on the oxidation activity of precious metals used in vehicle exhaust catalysts," *Applied Catalysis B: Environmental,* vol. 16, pp. L101-L104, 3/27, 1998.

[63] P. Hurtado, S. Ordonez, H. Sastre and F. V. Diez, "Combustion of methane over palladium catalyst in the presence of inorganic compounds: inhibition and deactivation phenomena," *Applied Catalysis B: Environmental,* vol. 47, pp. 85-93, 1/28, 2004.

[64] M. Aryafar and F. Zaera, "Kinetic study of the catalytic oxidation of alkanes over nickel, palladium, and platinum foils," *Catalysis Letters,* vol. 48, pp. 173-183, 1997.

[65] R. Burch and P. K. Loader, "Investigation of Pt/Al2O3 and Pd/Al2O3 catalysts for the combustion of methane at low concentrations," *Applied Catalysis B: Environmental,* vol. 5, pp. 149-164, 12/31, 1994.

[66] K. Everaert and J. Baeyens, "Catalytic combustion of volatile organic compounds," *J. Hazard. Mater.,* vol. 109, pp. 113-139, 6/18, 2004.

[67] W. B. Li, J. X. Wang and H. Gong, "Catalytic combustion of VOCs on non-noble metal catalysts," *Catalysis Today,* vol. 148, pp. 81-87, 10/30, 2009.

[68] W. R. May and E. A. Hirs, "Catalyst for improving the combustion efficiency of petroleum fuels in diesel engines," in *11th Diesel Engine Emissions Reduction Conference,* 2005, pp. 1-16.

[69] G. T. Linteris, M. D. Rumminger and V. I. Babushok, "Catalytic inhibition of laminar flames by transition metal compounds," *Progress in Energy and Combustion Science,* vol. 34, pp. 288-329, 6, 2008.

[70] S. Cimino, R. Pirone and L. Lisi, "Zirconia supported LaMnO3 monoliths for the catalytic combustion of methane," *Applied Catalysis B: Environmental,* vol. 35, pp. 243-254, 1/25, 2002.

[71] V. V. Lissianski, P. M. Maly, V. M. Zamansky and W. C. Gardiner, "Utilization of iron additives for advanced control of NOx emissions from stationary combustion sources," *Ind Eng Chem Res,* vol. 40, pp. 3287-3293, 2001.

[72] K. K. Akurati, A. Vital, G. Fortunato, R. Hany, F. Nueesch and T. Graule, "Flame synthesis of TiO2 nanoparticles with high photocatalytic activity," *Solid State Sciences,* vol. 9, pp. 247-257, 0, 2007.

[73] K. Buyukhatipoglu and A. Morss Clyne, "Controlled flame synthesis of aFe2O3 and Fe3O4 nanoparticles: effect of flame configuration, flame temperature, and additive loading," *J Nanopart Res,* vol. 12, pp. 1495-1508, 2010.

[74] K. B. Kim, K. A. Masiello and D. W. Hahn, "Reduction of soot emissions by iron pentacarbonyl in isooctane diffusion flames," *Combust. Flame,* vol. 154, pp. 164-180, 7, 2008.

[75] S. Li and X. Wei, "Promotion of CO oxidization and inhibition of NO formation by gaseous iron species during high-temperature off-gas combustion," *Energy Fuels,* vol. 25, pp. 967-974, 2011.

[76] H. Ma and H. Yang, "Combustion synthesis of titania nanoparticles in a premixed methane flame," *J. Alloys Compounds,* vol. 504, pp. 115-122, 8/13, 2010.

[77] G. T. Linteris, V. R. Katta and F. Takahashi, "Experimental and numerical evaluation of metallic compounds for suppressing cup-burner flames," *Combust. Flame,* vol. 138, pp. 78-96, 7, 2004.

[78] G. T. Linteris, M. D. Rumminger, V. Babushok and W. Tsang, "Flame inhibition by ferrocene and blends of inert and catalytic agents," *Symp Int Combust,* vol. 28, pp. 2965-2972, 2000.

[79] I. E. Gerasimov, D. A. Knyazkov, A. G. Shmakov, A. A. Paletsky, V. M. Shvartsberg, T. A. Bolshova and O. P. Korobeinichev, "Inhibition of hydrogen–oxygen flames by iron pentacarbonyl at atmospheric pressure," *Proceedings of the Combustion Institute,* vol. 33, pp. 2523-2529, 2011.

[80] R. E. A. Heyes and S. Kolaczkowski, *Introduction to Catalytic Combustion.* Canada: Gordon and Breach Science Publishers, 1997.

[81] R. E. Hayes, *Catalytic Combustion Kinetics : Using a Direct Search Algorithm to Evaluate Knetic Parameters from Light-Off Curves.* Quebec,Canada: GERAD, École des hautes études commerciales, 2002.

[82] J. J. Spivey, *Catalysis.* UK: Royal Society of Chemistry, 1999.

[83] M. Frenklach, H. Wang, C. -. Yu, M. Goldenberg, C. T. Bowman, R. K. Hanson, D. F. Davidson, E. J. Chang, G. P. Smith, D. M. Golden, W. C. Gardiner and V. Lissianski, "http://www.me.berkeley.edu/gri_mech/," .

[84] A. E. Lutz, "A numerical study of thermal ignition," Sandia National Laboratories, Tech. Rep. Technical Report SAND88-8228, 1988.

[85] M. D. Smoke and V. Giovangigli, "Formulation of the premixed and nonpremixed test problems," in *Reduced Kinetic Mechanisms and Asymptotic Approximationsfor Methane-Air Flames*, M. D. Smoke, Ed. Springer Berlin Heidelberg, 1991, pp. 1-28.

[86] J. Huang, P. G. Hill, W. K. Bushe and S. R. Munshi, "Shock-tube study of methane ignition under engine-relevant conditions: experiments and modeling," *Combust. Flame,* vol. 136, pp. 25-42, 1, 2004.

[87] R. K. Cheng and A. K. Oppenheim, "Autoignition in methane hydrogen mixtures," *Combust. Flame,* vol. 58, pp. 125-139, 11, 1984.

[88] M. Frenklach and D. E. Bornside, "Shock-initiated ignition in methane-propane mixtures," *Combust. Flame,* vol. 56, pp. 1-27, 4, 1984.

[89] D. Woiki, M. Votsmeier, D. F. Davidson, R. K. Hanson and C. T. Bowman, "CH-radical concentration measurements in fuel-rich CH4/O2/Ar and CH4/O2/NO/Ar mixtures behind shock waves," *Combust. Flame,* vol. 113, pp. 624-626, 6, 1998.

[90] V. P. Zhdanov, "Impact of surface science on the understanding of kinetics of heterogeneous catalytic reactions," *Surf Sci,* vol. 500, pp. 966-985, 3/10, 2002.

[91] C. Chou, J. Chen, G. H. Evans and W. S. Winters, "Numerical studies of methane catalytic combustion inside a monolith honeycomb reactor using multi-step surface reactions," *Combustion Sci. Technol.,* vol. 150, pp. 27-57, January 2000, 2000.

[92] Reaction Design, "CHEMKIN/CHEMKIN-PRO Getting started," 2010.

[93] Reaction Design:San Diego, "CHEMKIN-PRO 15101," 2010.

[94] Reaction Design, *CHEMKIN/CHEMKIN-PRO Theory Manual.* 2010.

[95] S. Mazumder and M. Grimm, "Numerical investigation of radiation effects in monolithic catalytic combustion reactors," *International Journal of Chemical Reactor Engineering,* vol. 9, 2011.

[96] L. R. Petzold, "A description of DASSL: A differential/algebraic system solver," Sandia National Laboratories, Tech. Rep. Technical Report SAND82-8637, 1982.

[97] Y. Zhang, J. Zhou, W. Yang, M. Liu and K. Cen, "Effects of hydrogen addition on methane catalytic combustion in a microtube," *Int J Hydrogen Energy,* vol. 32, pp. 1286-1293, 6, 2007.

[98] K. Pan, "Experimental Studies on Iron-Based Catalytic Combustion of Natural Gas," 2013.

[99] P. Griffiths, D. Haseth and A. James, *Fourier Transform Infrared Spectrometry (2nd Edition).* John Wiley & Sons, 2007.

[100] Thermo Fisher Scientific Inc., "TQ Analyst User's Guide," 2007.

[101] Thermo Fisher Scientific Inc., "OMNIC User's Guide Version 8.0," 2008.

[102] R. J. Kee, J. A. Miller, G. H. Evans and G. Dixon-Lewis, "A computational model of the structure and extinction of strained, opposed flow, premixed methane-air flames," *Symp Int Combust,* vol. 22, pp. 1479-1494, 1989.

[103] K. Pan, H. Qi, A. Patro, H. Zhu, S. Xiong and J. Wen, "Characterization of a counter-flow laminar flame for studying natural gas catalytic combustion," in *Combustion Institute - Canadian Section,* 2013, .